A Two-Laser-Experiment for CTA FlashCam

Masterarbeit
am Institut für Astronomie und Astrophysik
der Mathematisch-Naturwissenschaftlichen Fakultät
der Eberhard Karls Universität Tübingen
zur Erlangung des akademischen Grades
Master of Science (M.Sc.)

vorgelegt von

Fabian Leuschner

Tübingen
Februar 2020

Eidesstattliche Erklärung

Hiermit versichere ich, Fabian Leuschner an Eides statt, dass ich gemäß des allgemeinen Teils der Studien- und Prüfungsordnung der Universität Tübingen für den Studiengang Physik mit akademischer Abschlussprüfung Master of Science (M.Sc.) vom 30. Juli 2013 die vorliegende Arbeit mit dem Titel

A Two-Laser-Experiment for CTA FlashCam

selbstständig verfasst habe. Ich habe keine anderen als die angegebenen Quellen und Hilfsmittel benutzt und alle wörtlich oder sinngemäß aus anderen Werken übernommenen Aussagen als solche gekennzeichnet. Weiter versichere ich, dass die Arbeit weder vollständig noch in wesentlichen Teilen Gegenstand eines anderen Prüfungsverfahren gewesen ist, dass ich sie weder vollständig noch in wesentlichen Teilen veröffentlicht habe, sowie dass das in Dateiform eingreichte Exemplar mit den eingereichten gebundenen Exemplaren übereinstimmt.

Tübingen, den 06. Februar 2020

Fabian Leuschner

Abstract

FlashCam is an innovative camera for Cherenkov telescopes. In particular, it is tailored for the Medium-Sized Telescopes of the future Cherenkov Telescope Array as well as for H.E.S.S.-CT5, the world's largest Cherenkov Telescope.

The response on light pulses of a length of several nanoseconds, which are typical for Cherenkov light due to a photon induced air shower, was not determined as of yet. The analysis of earlier measurements of such kind never extended the preliminary state. The present thesis describes an experimental setup to probe such long-lasting pulses, using two lasers which are fired with a temporal delay. The functionality of this setup was validated in various measurements.

Using optical filters and a continuous, neutral-density filter-wheel, several measurement scenarios were performed in the framework of this thesis. They differ in the total intensity of the light pulses, as well as in the intensity of the pulses relative to each other.

During the analysis of these measurements it was achieved to discover several bugs and issues in the current, as well as in the recently developed analysis software. In an iterative process, most issues could be fixed and further improvements were suggested. After first improvements by the software developer, other, remaining issues were identified and suggestions were made how to correct for them.

Finally, ideas were sketched how to apply the presented setup in teaching, namely in a laboratory course for students who plan to specialize in astronomy and astrophysics.

Contents

I. Introduction and Physical Background

Astronomy is one of the oldest sciences of mankind. Until the nineteenth century, visible light was the only possibility to observe the night sky. Growing understanding of the physics of light and technological progress have opened up new ranges of wavelengths for astronomers. Each range led to the discovery of new phenomena and a more accurate picture of the universe. Starting in the 1980s, the TeV-band was opened by Cherenkov telescopes. Since these days more than one hundred sources were found, using the Imaging Air Cherenkov Technique. With the upcoming Cherenkov Telescope Array, scientists expect to find more than a thousand new ones [Ach13].

I.1. The Cherenkov Telescope Array

The Cherenkov Telescope Array (CTA) is the largest collaboration in ground-based gamma-ray astronomy worldwide. As of now, more than 1400 people from more than 30 countries work on the project. In 2025, when construction will be completed, more than 100 Cherenkov telescopes will be operated at the two telescope sites in Chile and on the Canary Island La Palma. Three different types of telescopes will be in use: Small-, Medium- and Large-Sized Telescopes (SST, MST and LST) to cover a broad energy range from 20 GeV up to 300 TeV.

This section will first summarize how Cherenkov astronomy works (Section I.1.1). Afterwards, in Section I.1.2, the CTA project goals will briefly be presented. Finally, Section I.1.3 is dedicated to the telescopes and the array layout.

I.1.1. Cherenkov Astronomy

Air showers and Cherenkov radiation

When a particle with an energy $E > 1\,\mathrm{GeV}$ hits the earth atmosphere, it initiates a so-called extended air shower. In multiple collisions, secondary particles are produced which either interact with the atmosphere or decay, producing new particles [Lon11].

Two types of showers can be distinguished: hadronic and pure electromagnetic. Hadronic showers are initiated by a hadron, typically a proton but also heavier nuclei up to iron. Such showers consist of multiple kinds of particles such as electrons, pions or muons [Lon11]. However, for CTA and similar observatories these showers merely form background for measurements where their multi-core-structure allows comparably easy discrimination [Aha04].

Electromagnetic showers are initiated by photons and electrons.[1] When a photon with an energy $E_0 > 1.22\,\mathrm{MeV}$ hits the atmosphere it can interact, undergoing pair-production[2] [Len12] after an average distance R. Following [Lon11] the resulting electron-positron pair moves through the atmosphere, with each particle on average carrying half

[1] Electrons form an inevitable background. However, this background is homogenous distributed over the sky and therefore does not disturb the observation of individual sources

[2] The difference of this figure compared to the 1 GeV above is due to nomenclature: 1.22 MeV is the threshold energy for pair production, while it needs a significant higher energy to speak of an extended air shower.

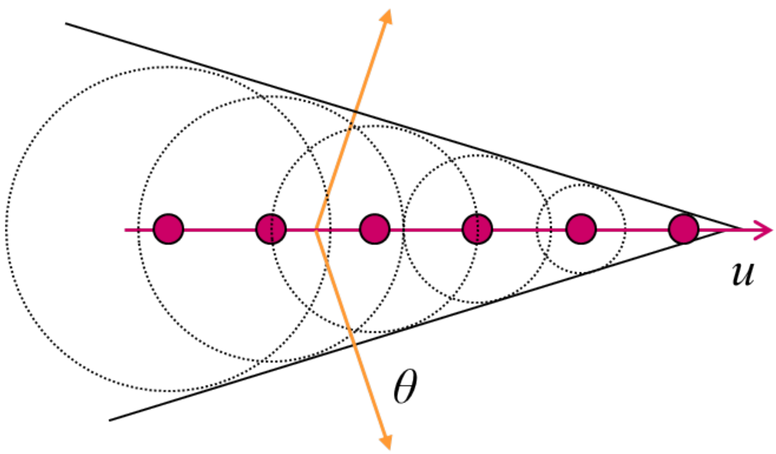

Figure I.1.: Propagation of wave fronts generated by a charged particle moving faster than the phase velocity of light in the surrounding medium. Image: [Sta14]

the energy of the initial photon, being $E_0/2$. After the distance R they in turn emit a photon via bremsstrahlung, carrying energy $E_0/4$. So after distance $2R$, there are one electron, one positron and two photons, each with energy $E_0/4$. This process is continued until the energy becomes too low for pair production.

The explanation of the Cherenkov effect follows [Ryb04]. At lower altitudes the atmosphere becomes more dense and the refractive index n increases. This leads to a reduced phase velocity of light $c_\mathrm{n} = \frac{c}{n}$. The electrons in the shower described above are highly relativistic, moving with velocities v close to the vacuum speed of light. So called *Cherenkov radiation* is emitted when I.1:

$$c_\mathrm{n} < v < c \tag{1}$$

is fulfilled. In Figure I.1 the red dots denote consecutive positions of a charged particle, moving from the left to the right. The circles around them are so-called *information spheres* caused by the moving charge at its respective position. These information spheres move outwards with the phase velocity of light $\frac{c}{n}$ and are therefore slower than the charged particle's forward movement. The information they carry is the potential of the charged particle, sent out from the corresponding position. Therefore, space is divided into two regions, one being inside and the other one being outside the so-called Cherenkov cone. There is no potential created by the moving charge at any point in space(time) outside the Cherenkov cone. However, at every point inside the cone, the potential of the charged particle sent out from two different positions is present[3]. This leads to asymmetric dipole polarization of the medium inside the cone radiating into the direction of motion of the charged particle [Wat11]. This radiation is called Cherenkov radiation. It is confined within the cone in spacetime. The opening angle α of the Cherenkov cone is defined by

$$\cos(\alpha) = \frac{c}{vn}. \tag{2}$$

A typical value of the opening angle is $\alpha = 1°$[Aha04]. Since the maximum of the shower development is about 10 km above sea level (a.s.l.), the radius of the cone in the optimal observing altitude (2 km a.s.l.) is about 120 m [Aha04]. Of course, these values depend on the velocity of the e^+/e^- and therefore on the energy of the initial

[3]This must be treated equally to interaction of the potentials of two independent, but equal charges.

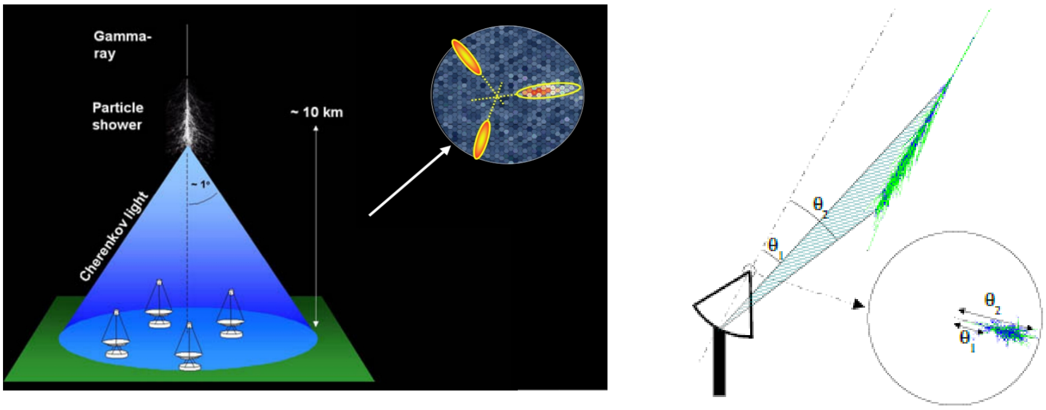

(a) Image: [ISD18]

(b) Image: [de 15]

Figure I.2.: Left: Pattern of an electromagnetic shower on a Cherenkov camera together with the reconstruction of patterns by other cameras in the same array. Right: Schematics of projecting an electromagnetic cascade into a Cherenkov telescope.

particle. The detectable Cherenkov radiation inside the cone is emitted in a time window of only a few nanoseconds. The spectrum of the flash peaks in blue to near-ultraviolet wavelengths.

Observation of Cherenkov radiation

To observe the phenomena described above, the Cherenkov telescopes of CTA use the *Imaging Air Cherenkov Technique* (IACT). Figure I.2 should be taken into account for a better understanding of the technique. The Cherenkov flash is projected as an ellipse on the camera, depending on the telescope position relative to the shower. The major axis of the ellipse (its length and orientation) allows reconstructing the direction to the origin of the initial photon.

With a single telescope an angular resolution of $14'$ is reachable [Kre98]. The accuracy can be significantly increased by using arrays of multiple telescopes. This is displayed in Figure I.3, where the angular resolutions of CTA and other very high energy astronomy missions are plotted. Further, an array allows improved background rejection.

Another advantage of using large arrays of Cherenkov telescopes is the increased effective area. The photon flux of astronomical sources usually follows a power-law with photon index ~ 2. Therefore, the flux at TeV-energies is extremely low[4]. Further, only a small number of photons is produced in one shower ($\sim 100\,\mathrm{m}^{-2}$ in a shower initiated by a 1 TeV photon [Aha04]). To detect more events and sources, one has to increase the area on ground covered by the arrays.

I.1.2. Goals of CTA

As mentioned at the very beginning, one of the goals of CTA is to increase the number of known gamma sources by an order of magnitude. Following [CTA19b], CTA will be innovative for its field from other aspects as well: it will be the first open observatory for gamma rays, accepting proposals not only from member institutions but also from the

[4] I.e. is the diffuse photon flux in the universe at 1 TeV of about $10^{-4}\,\mathrm{erg\,cm^{-2}\,s^{-1}\,sr^{-1}}$ [Hal02].

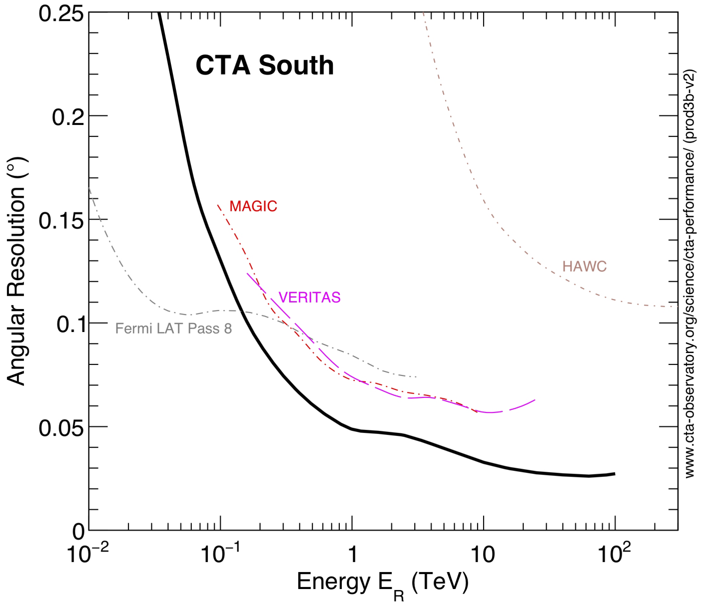

Figure I.3.: Angular resolution of CTA (south, simulated) in comparison to other GeV and TeV experiments. In its key energy range (0.15-5 TeV) CTA shows a vastly increased performance compared to any of the other experiments displayed. Image: [CTA19a]

whole scientific community. Beside that, about 40% of the observing time is dedicated to the so-called *Key Science Projects* (KSPs). There are three scientific topics on which CTA will concentrate: *Understanding the Origin and Role of Relativistic Cosmic Particles*, *Probing extreme environments* and *Exploring frontiers in physics*. On each of these topics, three fundamental questions were asked. According to these questions, nine KSPs have been defined. Each of them shall have an massive impact on at least one of the questions and will ideally help answering even more. Additionally, the *Dark Matter Programme* was founded. Its purpose is to understand the nature and distribution of Dark Matter in the universe. Research on the KSPs and the Dark Matter Programme will be performed as a set of observations examining different regions and energy bands. A detailed overview of the projects and especially the KSPs is given in [CTA19b], which at the same time is the source for the information presented in this section. The whole book is available as a free download on the project website [CTA19a].

I.1.3. Technology of CTA

CTA will consist of two arrays, one on the Canary island La Palma on top of the mountain Roque de los muchachos and the other one in Chile at the ESO Paranal-site. The plans for the two CTA sites are shown in Figure I.4. To achieve the ambitious goals, the knowledge gathered during precursor projects such as H.E.S.S. was combined with new developments. As mentioned at the beginning of this section, three differently sized telescopes will be constructed to cover the energy range from 20 GeV up to 300 TeV. Figure I.5 illustrates which energies will be covered by which telescope type(s).

In both arrays, four *Large-Sized Telescopes* (LSTs) will be placed in the center in a diamond-shaped arrangement. Due to their large mirrors (370 m^2 effective area) they are able to detect even the faint showers initiated by photons with energies down to 20 GeV.

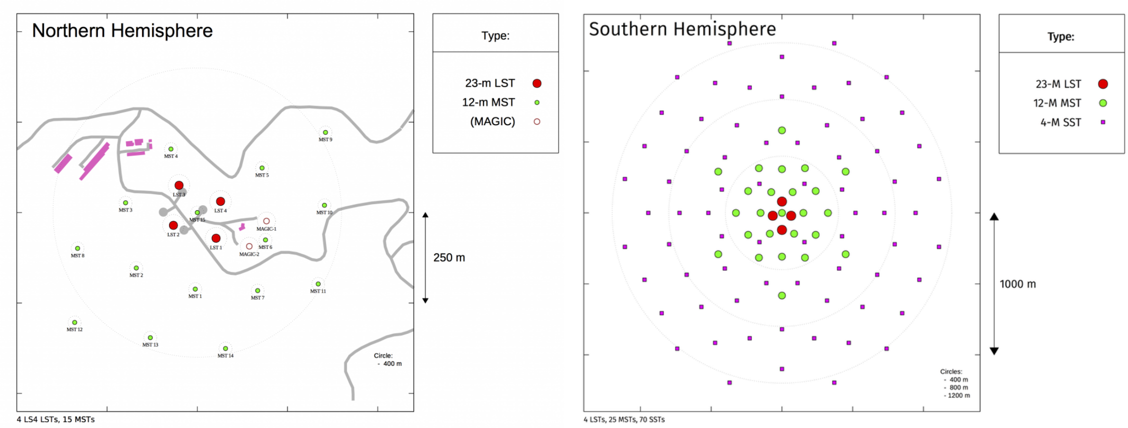

Figure I.4.: Current plans for the two CTA sites; Left: Roque de los Muchachos, La Palma, Spain. Right: Atacama desert, Chile. While in the southern array, all three telescope types will be constructed, in the northern array there will only be LSTs and MSTs. Mass production of telescopes and subsequently array construction is planned to start in 2021. Images: [CTA19a]

The LSTs are surrounded by Medium-Sized Telescopes (MSTs) with an effective mirror area of 12 m^2 each. They will be able to detect photons with energies between 80 GeV and 50 TeV, while full system sensitivity is provided from 150 GeV to 5 TeV covering the core energy range of CTA. Therefore, the MSTs are also known as the workhorses of CTA. In total, forty MSTs will be built. Fifteen will be operated in the northern array and twenty-five in the southern array. Those in the southern array are planned to be equipped with FlashCam, the camera which is the topic of this thesis.

In the southern array, there will also be Small-Sized-Telescopes (SSTs, effective mirror area of 8 m^2) to observe photons up to 300 TeV. The SSTs have smaller mirrors, since the showers initiated by those very high energetic photons are very bright. However, they are spread over a large area ($> 3\,km^2$) as displayed in Figure I.4. As mentioned above, the flux of most sources and subsequently of photons reaching earth in general follows a power-law with photon index ~ 2 and is therefore very small at highest energies. Therefore, the SSTs must cover a larger area as the LSTs and the MSTs to ensure they observe numerous showers. All the information presented in this section is taken from [CTA19a].

I.2. FlashCam

FlashCam is a camera for Cherenkov telescopes. A special focus is set on implementation into the MSTs of CTA. It follows an innovative approach of fully digital signal processing and triggering. The camera design is tailored to be in use under harsh environmental conditions such as in the Chilean Atacama desert. After intensive testing and performance verification in the MST structure prototype in Berlin-Adlershof and in a laboratory at the Max-Planck Institut für Kernphysik in Heidelberg (MPIK), a fully functional advanced prototype was installed as NamCam to the 28 m-telescope of the H.E.S.S.-experiment in Namibia in October 2019 and detected its first light in the night from October 22 to 23 [HES19].

When being in regular observing mode, experiences including but not limited to the camera performance and the developed in-field calibration will be acquired that will prove valuable for further improvements and performance verification.

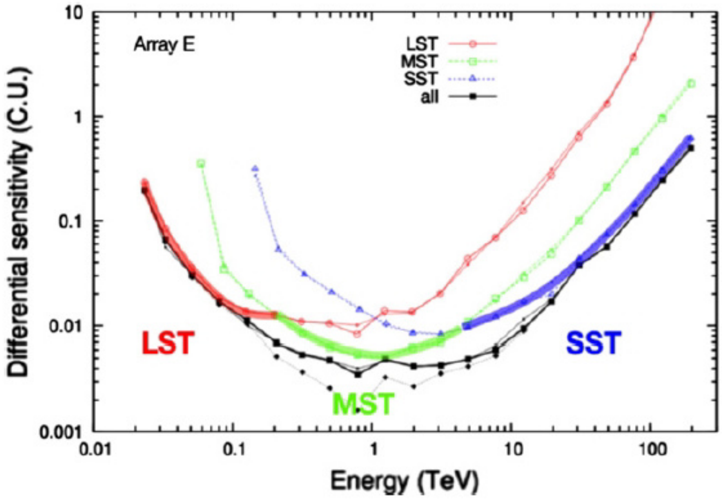

Figure I.5.: Differential sensitivity by telescope classes of CTA in units of the Flux of the Crab Nebula (50 h observation time, 5σ). The thick lines show the key energy range of the telescopes. Thin lines with small symbols illustrate the limited impact of a reduced dynamic range of the readout electronics. The dashed black line shows the overall sensitivity if there was no electron background [Ach13]. Image: [Ach13]

Section I.2.1 is dedicated to photo-electron multiplier tubes (PMTs), the current photo-detectors of FlashCam. Section I.2.2 will describe the camera and its readout electronics, mainly based on [Pue19] and [Pue15]. In Section I.2.3 the signal reconstruction and its dependence on the signal amplitude will be explained.

I.2.1. Photo-electron Multiplier Tubes

Photo-electron multiplier tubes (PMTs) are extremely sensitive light detectors. They provide an electric current that is proportional to the light intensity. PMTs are sufficiently sensitive to detect even single photons.

Figure I.6 shows how a PMT is constructed and serves to explain its principle. Behind the entrance window, there is a photo-cathode with a focusing grid directly behind. At the far end of the tube the corresponding anode is located. In between, there are multiple dynodes with increasingly high negative voltage. Inside the tube, there is a vacuum to eliminate the risk of electric discharges and to prevent the electrons from scattering.

A photon passing the entrance window may cause the photo-cathode to emit one photo-electron (p.e.). The high voltage will accelerate this electron towards the anode. Focused on the first dynode by the focusing grid, the photo-electron might hit it, producing secondary electrons that usually hit the second dynode, producing even more electrons leading to a cascading effect. At the anode the macroscopic current of these electrons will form the output signal. Since the number of electrons is proportional to the number of photo-electrons, which itself is proportional to the number of initial photons and therefore the light intensity, the output current is proportional to the light intensity. The gain of a PMT is of the order of $10^5 - 10^7$, depending on the number of dynodes and the applied high voltage.

However, there are two restricting parameters. One being the quantum efficiency[5]

[5]The ratio between incoming photons and produced photo-electrons

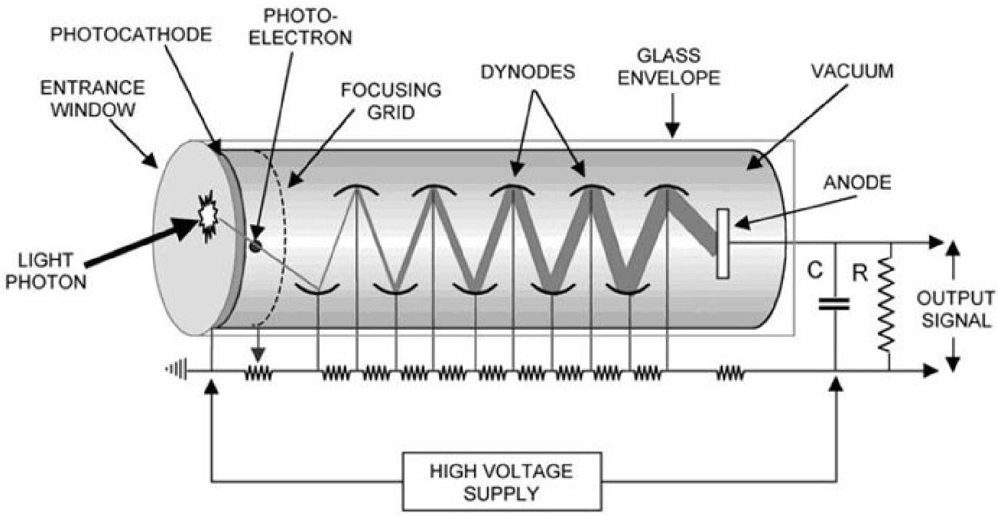

Figure I.6.: Sketch of a PMT. The number of dynodes may vary. I.e. for FlashCam in CTA, PMTs with seven dynodes will be used. Image: [SEN19]

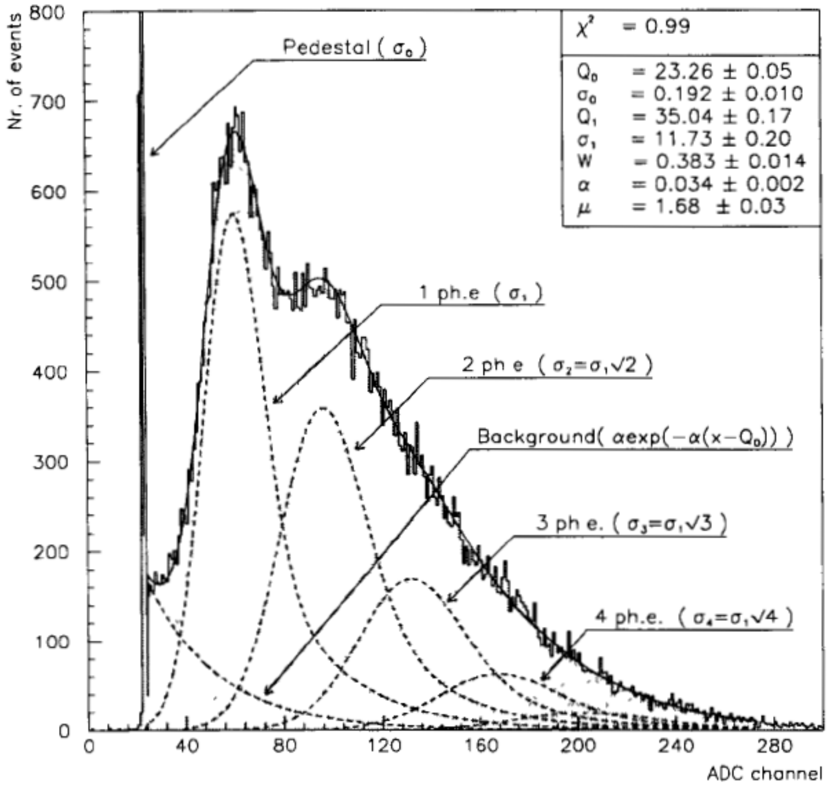

Figure I.7.: SPE spectrum with fitted response function (solid line) and its components (dashed lines). The total gain is the Q_1-parameter, multiplied with the ADC-channel width in units of the elementary charge (here: $1.560 Q_1 \cdot 10^6\,\mathrm{e}^{-1}$). Image: [Bel94]

(QE), the other being the p.e. collection efficiency[6] (CE). Since astronomy with the IACT started, and especially during the last decade, these two parameters could be increased. Modern PMTs have a p.e. CE of about 95%[7] and a QE $\sim$ 40%[8]. Therefore, total detection efficiency[9] (DE) has almost doubled during the past 20 years from little over 20% to, in best case, more than 40%.

To understand a setup using PMTs it is crucial to know its gain. The commonly used method are single photo-electron measurements (SPE measurements). If on average one p.e. is produced per detected event, the histogram of the reconstructed input charge follows the so-called PM-response function[10], which is derived in detail by [Bel94]. Its explanation is beyond the scope of this thesis. What is relevant here is that by fitting the response function on an SPE spectrum, the gain as one of the function parameters can be determined. It is given by the parameter $Q1$, which indicates the distance between the noise-peak (*pedestal*) and the first p.e.-peak. An example for such a spectrum together with the fitted PM-response function is displayed in Figure I.7.

Nevertheless, PMTs are no perfect instruments. Most importantly, they are expensive with unit costs of about 1500 EUR. Further, when operated in Cherenkov telescopes there is a gain-drift due to the night-sky background (NSB). This complicates quantitative event reconstruction, since it is almost not feasible to exactly determine the NSB-level. However, the gain-drift can be mostly corrected for on software basis. In other applications, such as particle physics there are further problems. I.e. PMTs must be built in such a way that they can withstand the pressure gradient generated by the vacuum inside them. Therefore, spacing between the single pixels is inevitable. It shall also be mentioned again that the DE still is below 50%.

A solution to these issues could be silicon photo-multipliers (SiPMs). These relatively new devices[11] are cubic, recently also hexagonal, small and unproblematic to handle. However, there are still issues concerning crosstalk and noise which have not yet been satisfactorily resolved. Further, they are still relatively slow. Furthermore, they are sensitive in redder wavelengths than PMTs, which results in a higher sensitivity to NSB. Nevertheless, Schwarzschild-Couder mounted telescopes such as SSTs can and will use SiPM-based cameras. In FlashCam, PMTs will be initially used as a well approved technology. However, efforts will be taken to make SiPMs usable for FlashCam in the future.

I.2.2. Camera Design and Architecture

As described in Section I.1.1, cameras for Cherenkov telescopes must be able to detect extremely faint light flashes on timescales of a few nanoseconds. The FlashCam team achieved to build such a camera with fully digital signal processing and dead-time free operation. Key building blocks are the photon detector plane (PDP), the readout electronics (ROS) and the data acquisition system (DAQ), with connections structured as shown in Figure I.9. The spatial layout of the whole camera is shown in Figure I.8. Since these building blocks are independent of each other and consist of independent modules themselves the term *horizontal architecture* is used often.

A camera as shown in Figure I.8 has dimensions of $2.9 \times 3.0 \times 1.1$ m. It consists of an outer housing (*camera insulation case with rear door* and the *front plate with lid system*)

[6] The ratio between produced photo-electrons and detected signals
[7] Compare to 85% in the 2000s
[8] A significant increase, compared to 25% in the early and at most 34% in the late 2000s
[9] The product of QE and p.e. CE
[10] Although in the framework of this thesis only PMTs are used the function also applies to other photo-multipliers (PMs), i.e. SiPMs.
[11] First developments started in Moscow in 1989.

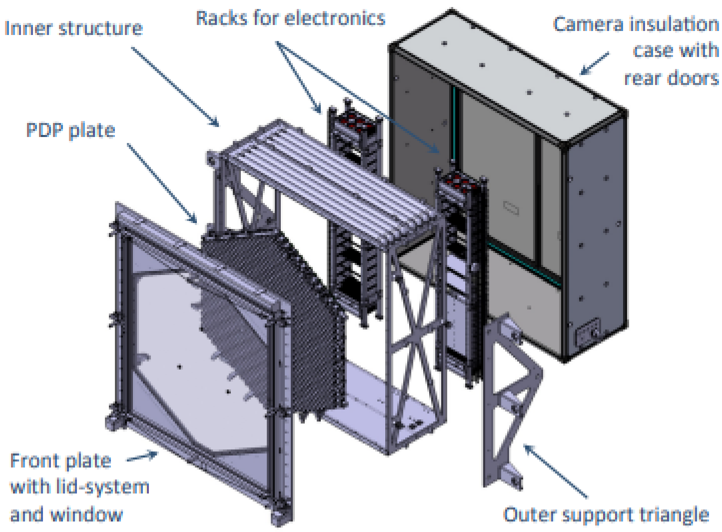

Figure I.8.: Computer-aided-design sketch of a FlashCam. The outer dimensions are $2.9 \times 3.0 \times 1.1\,\mathrm{m}^3$. Image: [Pue15]

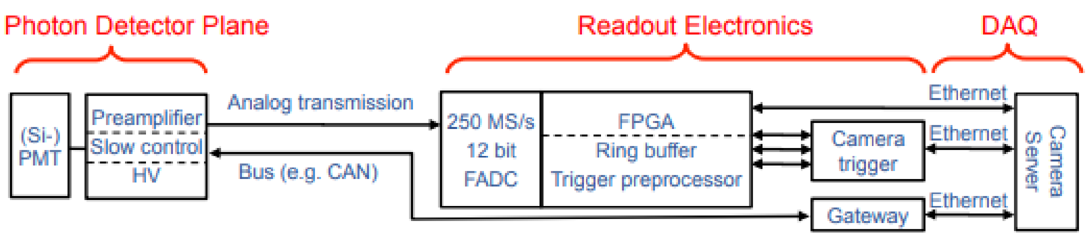

Figure I.9.: Basic building blocks of the FlashCam signal chain. Image: [Pue15] to protect the electronic devices from environmental impacts. Beside a safety cabinet inside, dry air overpressure keeps humidity low and avoids dust to enter the camera body, which is essential for operation in the desert. Further, a water cooling system dissipates the heat produced by the electronics. The lid on the front plate protects the PDP from daylight and serves as an additional cover in case of precipitation. The front plate itself is made of plexiglass and prevents photons with wavelengths below 300 nm to enter the camera.

Inside the housing, the *inner structure* is fixed with the *outer support triangles* to the insulation case. The inner structure carries the *PDP plate* and the *racks for electronics*. These electronics mainly consist of the readout electronics but also include the safety cabinet and the regulating systems described above.

The PDP as well as readout electronics follow a highly modular concept. The PDP contains 1758 pixels, structured in 147 PDP-modules. Each PDP-module hosts twelve pixels[12] and includes high-voltage (HV) supply, slow control and preamplifiers, as Figure I.9 shows. The PMTs are arranged in a hexagonal structure with 50 mm pixel spacing. Winston cones are used to fill up this space and to ensure that only photons coming from the telescope mirror are detected. The gain of each pixel, determined by the HV applied to the PMT, can be set individually. The used preamplifiers amplify weak signals linearly and saturate for higher pulses in a controlled way[13]. This provides a dynamic range above 3000 p.e. but keeps sub-p.e. resolution for weak signals in a single channel.

In the ROS, the incoming analog signals are digitized with commercial 12-bit flash analog-to-digital converters (FADCs) at a rate of 250 MS s^{-1}. There are eighty-four FADC-modules, each serving either twelve or twenty-four pixels (so one or two PDP-modules). On each FADC-module, a field programmable gate array (FPGA) is mounted. The FPGA buffers digitized samples and processes them in a configurable way for trigger decisions. The default trigger scheme will be explained below.

When being triggered, waveforms of up to 15.6 µs length are read out to the camera server, being a standard commercial server. The servers of all FlashCams in an array are located at the array control. There, the raw traces are processed as described in Section I.2.1. An array-wide precision clock-distribution network[14] ensures that events observed by one telescope can be correctly assigned to those detected by other telescopes. Triggering is performed by special Trigger-modules. Each Trigger-module is responsible for seven FADC-modules. For default triggering patches of three pixels are formed in the FADC-modules by summing up the integrals over their traces. The sum of seven such patches (=21 pixels) is jointly considered in a Trigger-module. If it exceeds a certain threshold, the camera will be triggered. For the edge areas of each Trigger-module so-called trigger links transmit the information between neighboring Trigger-modules to make sure the corresponding patches can be properly formed. Following the idea of having a modular layout, the Trigger-modules are based on the same motherboard as the FADC-modules. There is also an FPGA mounted, which here is used to process the triggering.

Further, there is one Master-module, serving as interface between camera and camera-server, respectively the array-control and for triggering the whole camera if one Trigger-module triggers.

To achieve fast signal transmission, Ethernet cables are used to connect the PDP with the ROS. The analog signals coming from the PDP are transmitted via shielded, twisted

[12]The missing six pixels are due to mounting of the front plate (three) and due to masked pixels for calibration purposes (also three).

[13]The threshold is determined by the negative supply voltage of the PMTs

[14]Both CTA arrays will use a White Rabbit (WR) network.

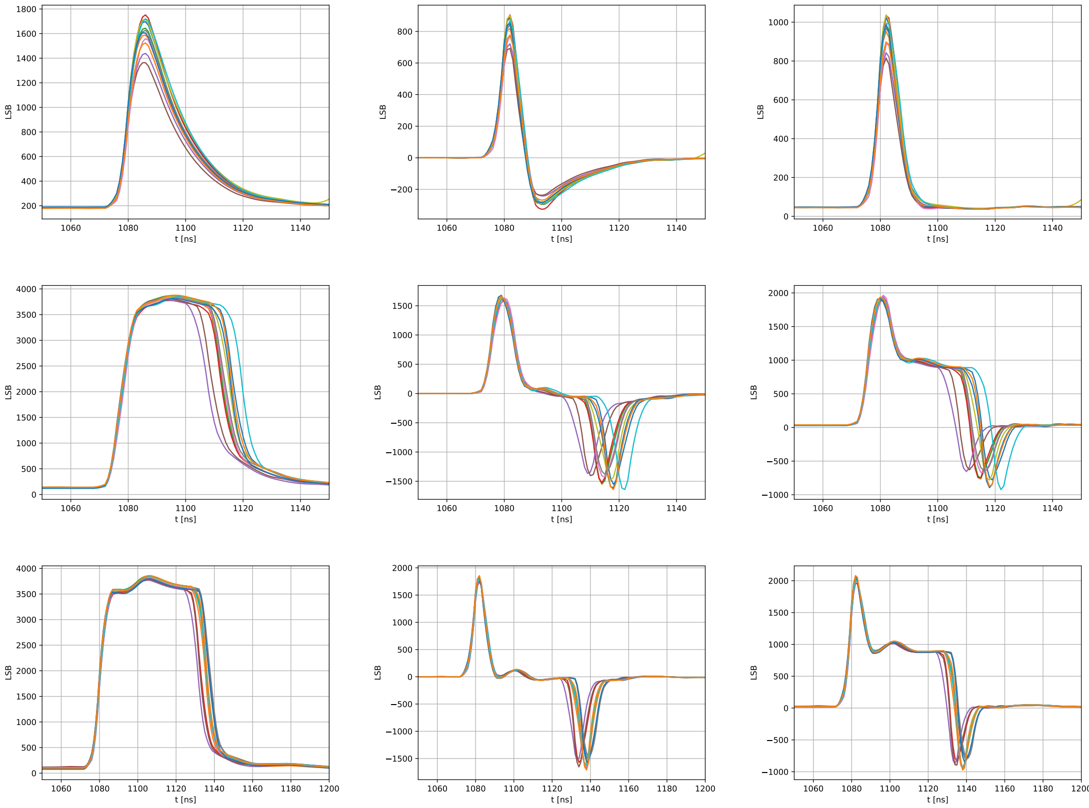

Figure I.10.: The plots show the three steps of digital signal processing in the different regimes. In the left column, upsampled traces are displayed, the center column shows differentiated traces and the right column contains pz-corrected traces. The data used for creating these plots was taken in linear regime for the top row, in transition regime for the middle row and in non-linear regime for the bottom row. The x-axis extends over 100 ns in the linear regime and the transition regime and over 150 ns in the non-linear regime. The values on the y-axis differ a lot, depending on the regime and the processing step. For all plots one event detected by twelve channels is displayed.

pair cat 6 cables to the ROS[15] to ensure there is no coupling in of noise. The connection between camera-server and Master-module is formed by four 10 Gbit Ethernet fibers.

To conclude: a FlashCam, equipped for an MST, consists of 1758 pixels in 147 PDP-modules. They are digitized on eighty-four FADC-modules, supplemented by twelve Trigger-modules, concluding with one Master-module and a server. The camera is protected by its housing against environmental impact. It operates dead-time free for event rates that can be larger than 35 kHz and samples with a rate of 250 MS s^{-1} [Pue15].

I.2.3. The Linear and Non-Linear Regime

The goal of camera internal signal processing is to reconstruct the number of photons and therefore the intensity captured by each pixel. With this figure, pattern as shown on the left picture of Figure I.2 can be formed. As mentioned in Section I.1.1 these pattern allow to derive the direction and energy of the initial photon and its source. Since the DE

[15] Four channels per cable

is known the challenging part remaining is to reconstruct the number of photo-electrons.

The preamplifiers are the only analog signal processing devices. The majority of signal processing is performed digital. The whole analog signal chain is DC-coupled. This ensures that the input signals are completely preserved, which, among other things, allows conclusions to be drawn about the NSB.

As mentioned above, the preamplifiers saturate at high signal amplitudes. Therefore, three different regimes for the reconstruction of the number of p.e. are introduced. The so-called *linear regime* and *non-linear regime* are comparable to the high- and low-gain signal chains of conventional detectors. Additionally, the *transition regime* was defined in between the two already mentioned. This section will give an introduction to the reconstruction and the different parameters used.

When the camera triggers a part of the data buffered in the FADC-modules is read-out to the camera server. The length (in samples of 4 ns) of these *traces* can be defined with the slow control and is by default 64 samples. The camera server then performs three steps of signal processing: *upsampling*, *differentiation* and *pole-zero-correction*.

Upsampling describes the process of artificially increasing the sampling rate by interpolation. For FlashCam the raw-data is sampled at a rate of 250 MHz. Default upsampling uses a factor of 4, leading to a sampling rate of 1 GHz. This is achieved via a two-step process: The raw data can be understood as a sequence of n values $x = [x_1, x_2, ...x_n]$. If the upsampling factor is u, each of these values will be randomly placed into a subsequence of $u - 1$ zeros: for $u = 4$, it might be $x_u = [[0, 0, x_1, 0], [x_2, 0, 0, 0], ..., [0, x_n, 0, 0]]$. In the second step the zeros are smoothed out by numbers interpolated from the values of the raw data. The found sequence x_u, with $n \cdot u$ values can be plotted. In FlashCam data analysis, the x-axis represents time, the unit of the y-axis is LSB (least significant bit). This shall be referred to as *upsampled trace*.

For *differentiation* the difference quotient of two neighboring points in the upsampled trace is formed. Again, one receives $n \cdot u$ discrete points, which can be plotted. Subsequently, it shall be referred to as *differentiated trace*. In hardware signal processing, the differentiated trace can be obtained by shaping the signal with a *CR Differentiator* circuit.[16]

The last step of the signal processing is the *pole-zero correction* (pz-correction). It is the digital representation of a *CR Differentiator with pole-zero cancellation* circuit, being a CR Differentiator with an additional, adjustable resistance that is added in parallel with the capacitor in the CR circuit. The resistor can be adjusted to cancel out the undershoot. In the mathematical representation, the poles of the differentiated trace, being the negative values in the differentiated signal, are replaced by zeros. This is the origin of the name of the circuit. In digital signal processing this mathematical operation is done in software and the adjustment of the resistor is replaced by configuration values [Ort20]. The resulting trace is called *pz-corrected trace*. Figure I.10 shows examples for each of the traces mentioned in the different regimes of FlashCam.

The acquired data is used for reconstructing the number of p.e. in one of the three regimes. At low intensities, the camera response is linear in amplitude and edge steepness, for a given input pulse shape. The corresponding reconstruction regime is accordingly called *linear regime*. Plots of traces in this regime are shown in the upper row of Figure I.10.

For reconstruction of the number of p.e. in the linear regime the maximum of the pz-corrected trace *pzmax* is used. It would be also possible to use the maximum of the upsampled trace *umax* (which was in discussion), however, *pzmax* is sharper and therefore more suitable. To find the reconstructed number of p.e. (pe_{rec}), *pzmax* is sub-

[16]This and the circuit mentioned in the following are shown in Appendix A.

tracted by the background of the measurement *pzbgmax* and divided by the gain of the pz-corrected trace *pzgain*, as stated in Equation 3. *pzbgmax* is defined as the local maximum of the pz-corrected trace in the sequence between 16 ns and 20 ns before the global maximum of the pz-corrected trace. *pzgain* must be determined separately in an SPE-measurement.

$$pe_{\text{rec,lin}} = \frac{pzmax - pzbgmax}{pzgain} \tag{3}$$

At higher amplitudes the preamplifiers saturate. The shape of the upsampled trace becomes nearly rectangular, as Figure I.10 shows. In this regime the maximum of the upsampled, as well as of the pz-corrected trace, is independent of the intensity of the photon detected. The reconstruction regime is referred to as *non-linear regime*. Plots corresponding to the three steps of signal processing in this regime are shown in the bottom row of Figure I.10.

However, the preamplifiers saturate in a controlled way. This means that they will elongate the duration of the signal at maximal amplitude. Hence, in the non-linear regime the duration of the signal can be used for reconstructing the number of p.e.. The duration is found by considering the distance between the maximum and the minimum of the differentiated trace, as shown in the right image of Figure I.11. This parameter is referred to as *width of the differentiated trace* w_d by the FlashCam team[17]. FlashCam was designed such that w_d depends logarithmically (with some offset) on the intensity. Therefore, reconstruction of the number of p.e. is done via a power law of w_d considering the offset given in Equation 4.

$$pe_{\text{rec,non}} = \frac{1}{ugain} \cdot \exp\left[c \cdot w_d + b_{\text{scale}} \cdot bl_{\text{shift}} + b_{\text{offset}}\right] \tag{4}$$

ugain is the gain of the maximum of the upsampled trace *umax* and can be determined in an SPE-measurement, along with the already introduced *pzgain*. The offset and the index of the power law are given by several parameters: bl_{shift} is the shift due to the baseline and corresponds to a value set at the beginning of the measurement. c and b_{scale} are constants and b_{offset} is a pixel-wise factor. They have to be determined while calibrating the camera. It was found that the non-linear regime is divided into two sub-regimes (the limit depends on the gain and therefore on the HV applied to the PMTs). Both are following the same power-law but with different parameters. Therefore, in Appendix C two values each for c, b_{scale} and b_{offset} are given.

In between the linear and the non-linear regime, the *transition regime* was introduced. Plots of traces measured in this regime are shown in the center row of Figure I.10.

In this regime, the preamplifiers already saturate, therefore *pzmax* is not linear anymore. However, they do not sufficiently saturate that the dependency given in Equation 4 is valid. Therefore, the integral over the upsampled trace, subtracted by a baseline of 1200 LSB, A_{1200} is taken as the parameter for reconstruction. Numerically A_{1200} is formed by summing up all values forming the upsampled trace, subtracted by 1200. A visualization is given in the left plot of Figure I.11. The subtraction of the baseline is necessary to cancel out any possible background. The number of p.e. is then given by

$$pe_{\text{rec,trans}} = \frac{1}{ugain} \cdot (g_A A_{1200} + offset) \tag{5}$$

g_A is the gain of the area and must be calculated for each pixel depending on *pzgain*. *offset* is a constant, determined during calibration of the camera. *ugain* again is the gain

[17] In the software, it is also referred to as *dwidth*.

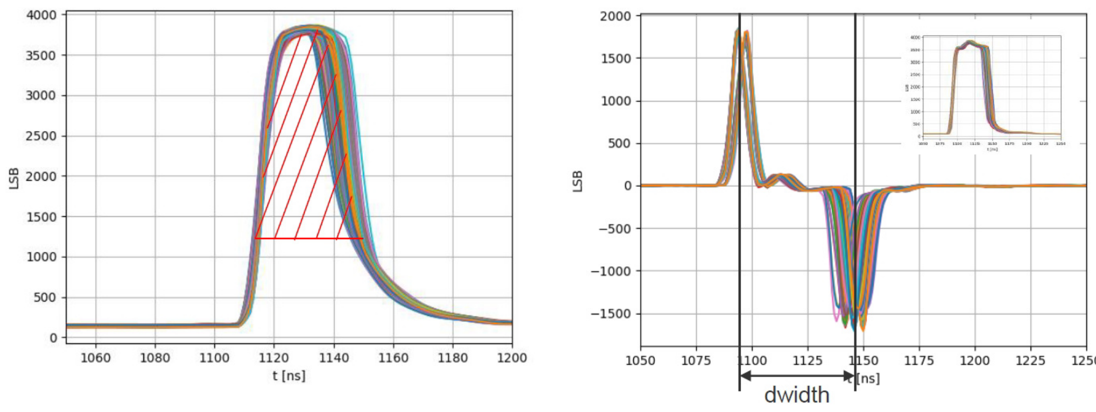

Figure I.11.: Left: Traces in transition regime (about 400 p.e.), with A_{1200} indicated in red. Right: Differentiated traces with markers for start and end (estimated) of w_{d}. In FlashCam analysis software, this parameter is usually labeled as *dwidth*. In the upper right corner of the right figure, the upsampled traces which lead to the differentiated traces are shown for comparison.

of the maximum of the upsampled trace *umax*.

At the edges of the transition regime, there are overlaps with the linear and the non-linear regime, respectively. These overlaps are used to first calibrate the parameters for transition regime reconstruction with the linear regime and afterwards the parameters of the non-linear regime with the transition regime.

In operational mode the overlap zones are used to achieve more accurate values by considering both adjacent regimes using a weighted average. The weights are defined so that they result in 1 when only the linear or non-linear regime shall be taken into account and 0 when only the transition regime shall be taken into account. The limits are defined as the upper limit of the linear regime and the lower threshold of the transition regime[18] for the transition from linear to transition regime. For the other overlap zone (transition to non-linear regime) the limits are the lower threshold of the non-linear regime and the upper limit of the transition regime[19]. The weights for the transition between linear and transition regime then are the defined by

$$W = \frac{2800\,\mathrm{LSB} - rmax}{2800\,\mathrm{LSB} - 2500\,\mathrm{LSB}} \tag{6}$$

with *rmax* being the maximum of the raw trace. For the transition from the transition regime to the non-linear regime the weights are defined by

$$W = \frac{w_{\mathrm{d}} - 20\,\mathrm{ns}}{45\,\mathrm{ns} - 20\,\mathrm{ns}} \tag{7}$$

Given in photo-electrons, the overlap zones roughly extend from 200 p.e. to 300 p.e. and from 500 p.e. to 600 p.e..

[18]Default: 2800 LSB and 2500 LSB as maximum of the raw trace, *rmax*

[19]Default: $w_{\mathrm{d}} = 20\,\mathrm{ns}$ and $w_{\mathrm{d}} = 45\,\mathrm{ns}$

II. FlashCam Two-Laser-Experiment

The goal of this thesis is to determine the response of FlashCam on light pulses of a length typical for gamma ray induced air showers. However, it is technically very challenging to create light pulses with freely tunable durations of several nanoseconds. As a good approximation for such light pulses an experiment with two lasers was set up. This setup will be described in the first part of this chapter, Section II.1. The second part, Section II.2, is dedicated to validation measurements for the experiment.

II.1. Setup

The FlashCam Two-Laser-Experiment was set up in the context of this thesis. It is based on an existing experiment at the Institut für Astronomie und Astrophysik Tübingen (IAAT), which was set up by M. Biegger in 2017. A short description of this setup is given in Section II.1.1. For more detailed information, see [Bie17]. In Section II.1.2, the Two-Laser-Setup itself is described, which comprises an optical setup inside a darkbox and electronics for controlling outside of it. While Section II.1.1 focuses primarily on the darkbox excluding the optical components, Section II.1.2 discusses all details in depth. Further information such as serial numbers of all devices mentioned are listed in Appendix B.

II.1.1. Existing FlashCam Test Setup

The following section is mainly based on Section 3.1 of [Bie17]. The test setup is located inside a darkbox with outer dimensions of $80 \times 80\,\mathrm{cm}^2$ in cross-section and 248 cm in length. The darkbox is constructed of black PVC-plates, held in place by aluminum-connectors and wrapped with black, non-reflecting tape on the inside. Its bottom is about 60 cm above the floor. It can be opened on one side over the whole length or alternatively on the right half of this side only, as shown in Figure II.1.

On the small ends of the darkbox two cable boxes are mounted. They allow cables to be routed into the darkbox for communication with electrical components inside. The cables can only be routed through small holes in the cable boxes and the PVC-plates of the darkbox. This is inconvenient to handle but it ensures as little contamination by external light sources as possible.

Inside the darkbox a simple "'One-Laser-Setup"' (in contrary to the Two-Laser-Setup of this thesis) is implemented. It consists of an optical bench[20] with an optical rail on top. The bench is mounted on an enhancement, about 25 cm above the bottom of the box. In the right half of the darkbox the enhancement can be moved longitudinally but not laterally. This ensures it to be centered with respect to the cross-section. On the optical rail a diffuser and a continuous, neutral-density (nd) filter-wheel, movable on 4096 steps with a servo-motor, are located. A laser mounted on the optical bench sends light through the filter-wheel towards the diffuser. This optical setup acts as a diffuse light source. More detailed information about all the components will be given in Section II.1.2, where the final setup shall be described.

[20] Area of $15 \times 60\,\mathrm{cm}^2$

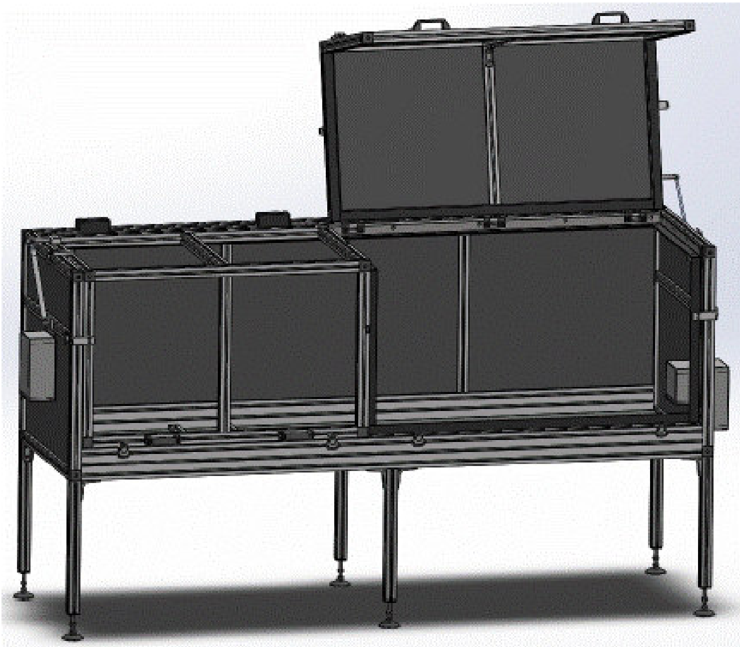

Figure II.1.: CAD-sketch of the darkbox. In this illustration the right side is opened while the left side remains closed. Clearly visible are the boxes allowing cable insertion. Image: [Bie17]

Underneath the optical bench a blue LED ($\lambda \approx 465\,\mathrm{nm}$) is installed to simulate night-sky background (NSB) illumination. A filter with optical density (od)[21] 4.0 is located in front of the LED to make the whole energy (and therefore dynamic) range, provided by the LED, usable for simulating different NSB-levels. Detailed information on the NSB-LED, its calibration and NSB-measurements in general can be found in [Sal18].

In the left half of the darkbox a mount for PDP-modules is installed. If available, it can be equipped with up to three modules allowing for 36 pixels detecting light coming from the source. However, throughout this whole thesis only one PDP-module and therefore 12 pixels are used. Each pixel is realized by an 8-dynode PMT. The ROS is placed outside the darkbox. The Ethernet cables for data transfer, as well as the HV supply cable are routed through the cable box on the left side of the darkbox. The ROS consists of a backplane, currently equipped with one FADC- and one Trigger-module. The number of FADC-modules could be increased if needed.

The light tightness of the darkbox was estimated. For the total of 12 photomultiplier-tubes a count rate of 62 events/s was found [Bie17]. Biegger attributed this rate to dark counts rather than actual photon events. Therefore, the box is considered as totally dark in the wavelength-regime of the PMTs.

Except for the laser, the setup is computer-controlled. This comprises the servo-motor, the NSB-LED and the PDP slow control as well as the readout of the ROS crate.

II.1.2. Upgrades for the Two-Laser-Setup

The Two-Laser-Setup is an expansion of the existing FlashCam test setup and developed in the framework of this thesis. The goal is to simulate light pulses of a length that is typical for Cherenkov flashes induced by air showers (up to 10 ns). To achieve this, two

[21]Optical density: if the intensity of light is changed, so that $I_{\text{final}} = a * I_{\text{initial}}$, the optical density is $\log_{10}(a)$

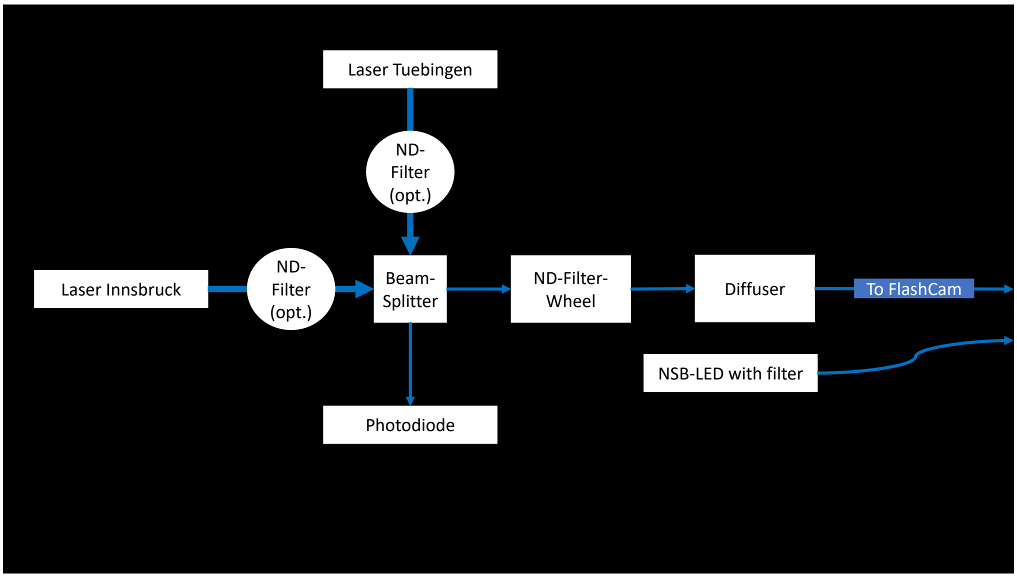

Figure II.2.: Schematics of the Two-Laser-Setup inside the darkbox.

pulsed lasers are fired with a temporal delay. For completeness of the measurement curves[22], delays of $0\,\text{ns} \leq \Delta t \leq 80\,\text{ns}$ were considered.

Inside the darkbox the existing optical setup was developed further. Now two lasers are placed in an angle of 90° relative to each other. Their light is split by a beam splitter cube at the same distance to each of the lasers. One of the exiting beams points towards a fast rising photo-diode (PD) used for monitoring the timing and the relative amplitude of the lasers. The PD sends intensity-dependent voltages[23] to an oscilloscope located outside the darkbox. The other beam goes – as in the initial setup – through the nd-filter-wheel and the diffuser towards the PDP-module. The filter-wheel is used to control the total intensity reaching the PDP-module. To change the relative intensities of the lasers readily, filters with fixed optical density can be added in front of each laser. A flowchart of the optical setup is shown in Figure II.2.

The originally used laser is property of the IAAT, the second one is a loan from the University of Innsbruck. Therefore, the former shall be referred to as *Laser Tuebingen*, the latter as *Laser Innsbruck*. Both are part of the *LDH-series* of the PicoQuant company from Berlin [Pic19]. An extract of the LDH-series data-sheet can be found in the appendix as Figure B.1. The serial number of Laser Tuebingen is *D-C-405*, the serial number of Laser Innsbruck is *P-C-440B*. According to the data sheet Laser Tuebingen sends out light with a wavelength of $\lambda_{\text{Tue}} = (405 \pm 10)$ nm, while for the light from Laser Innsbruck $\lambda_{\text{Inn}} = (440 \pm 10)$ nm is valid. To simulate the light pulses lasers are used instead of other light sources (such as e.g. LEDs), because their rise time is much faster[24] and the collimated light beam of a laser is more easy to handle.

The beam-splitter-cube has a transmission : reflectance-ratio of about 1:1. Diagrams plotting the transmission and reflectance as functions of the wavelength are shown in Figure B.2 in the appendix. The diffuser is transparent[25] for wavelengths between 380 nm and 1100 nm. It spreads collimated light with $\lambda = 633$ nm to a 20° cone. Only small deviations are expected for the light sources used ($\lambda \sim 400$ nm) [Bie17]. The nd-

[22] See Chapter III and Chapter IV

[23] These voltages will be referred to as *PD output*

[24] I.e. an LED-based calibration device has a pulse width of about 60 ns which is more than a hundred times as long as the pulse width of the used lasers.

[25] About 90% transmission

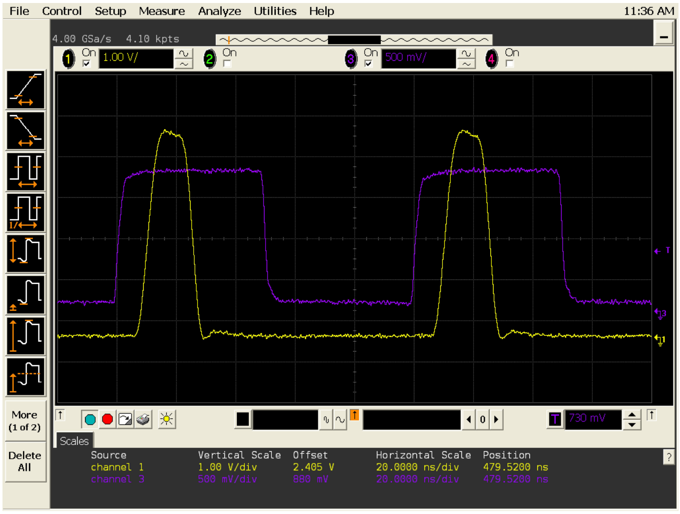

Figure II.3.: Waveforms of the two pulse-generator outputs. The output for triggering the lasers is plotted in yellow, whilst the Sync-output is in purple. The important feature of the curves is their length: the Sync-output lasts much longer than the other one.

filter-wheel reduces light in the optical regime[26] independent of its wavelength. The optical density is between 0 and 4.0. This corresponds to attenuations from a factor of 1 up to 10 000. Further information concerning the optical devices can be found on the manufacturer website [Tho19].

As with the One-Laser-Setup the controlling electronics is located completely outside the darkbox. Figure II.4 gives an overview of the devices and their connections. A pulse generator generates electric pulses with a frequency of 500 kHz which are used for triggering the whole setup. These trigger signals are split and sent through two individual delay-lines to the laser drivers. When triggered, they send out trigger pulses to the laser heads via uniform cables, leading to no additional delay. The delays in the delay-lines can be set via manual switches and are used to define the temporal delay between the firing of the two lasers. If all switches are set to OFF, the delay between the two laser pulses shall be referred to as *standard-delay* and Laser Tuebingen is fired 39 ns before Laser Innsbruck. When setting delays with the delay-line for Laser Tuebingen, the delay between the two lasers will decrease[27]. On the other hand, if additional delays in the delay-line for Laser Innsbruck are set, the delay will increase[28]. From now on, the delay set by these delay-lines shall be referred to as Δt. In Section II.2 measurements are presented to verify that the set delays correspond to real delays.

The second output of the pulse-generator – the so-called *Sync* – is used for triggering the oscilloscope (for the PD) and the ROS. The Sync-signal has the same frequency as the signal used to trigger the lasers (*output*) but another shape, as can be seen in Figure II.3: while the output sends a short gaussian pulse[29], the Synce sends a signal that is fast rising and in the first half the period ON, before going OFF for the other half. To be understood by the ROS, the signal has to be transmitted via an Ethernet cable.

Due to the form of the Sync-signal a first delay-line which delays the laser trigger-signal for ≈100 ns is necessary. If the laser trigger-signal was not delayed the signal

[26] $350\,\text{nm} \leq \lambda \leq 700\,\text{nm}$
[27] The trigger for Laser Tuebingen is shifted towards the (here fixed) trigger for Laser Innsbruck
[28] The trigger for Laser Innsbruck is shifted away from the (here fixed) trigger for Laser Tuebingen
[29] The deviations from that in Figure II.3 are due to mis-impedancies in the cables

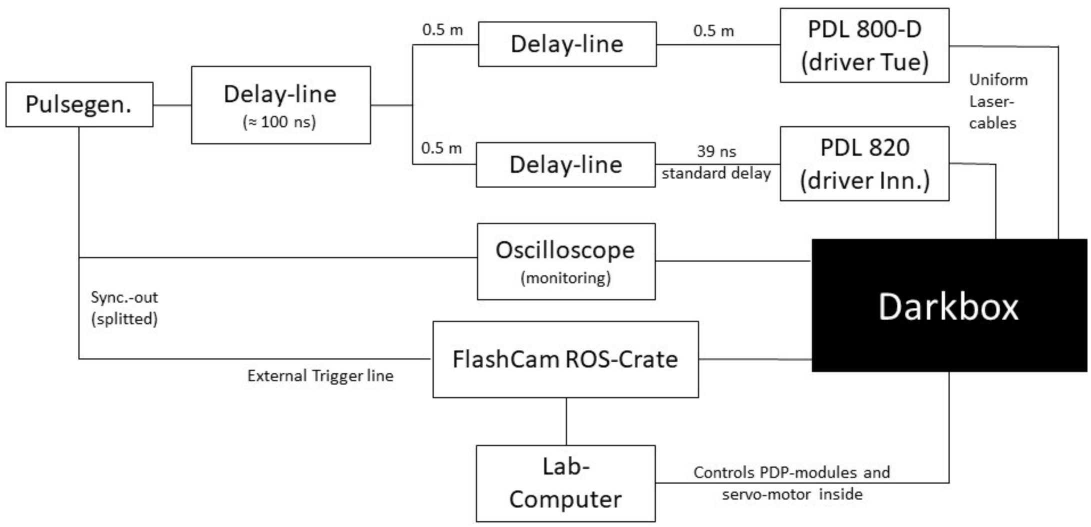

Figure II.4.: Schematics of the electronics outside the darkbox for the Two-Laser-Setup with connections for signal and data transfer.

from the PDP-module would reach the FADC-module while the trigger is still ON. In that case crosstalk in the ROS between trigger (from Sync) and signal (from the PDP-module) would be unavoidable.

After the light is detected by the PD and/or the PDP the resulting output-signals are sent to the oscilloscope (PD) and/or the ROS-crate (PDP-module), respectively. The oscilloscope is used for monitoring the setup. The PDP-module is the device producing the measurement data. Its signals can be saved on the laboratory computer after being processed in the ROS.

II.2. Validation Measurements

Before the measurements described in Chapter III and Chapter IV can be performed properly, the functionality of the setup must be validated. The following points have to be addressed:

- Proper delay-setting with the delay-lines needs to be confirmed.
- There should not be any reflections disturbing the measurements.
- The gain of the PDP-module (in the current setup) needs to be determined.
- It has to be verified, if varying the intensities with the laser drivers has the same effect on the system response as varying the intensities via the optical filters.

This section will discuss the practical implementation of the points above.

II.2.1. Confirmation of Delay-Setting

To confirm the delay-setting all switches of both delay-lines are tested once. This testing is performed as follows: For each measurement 25000 samples are recorded with the oscilloscope. It is verified if the delay set at the delay-lines corresponds to the average time difference measured between trigger and signal. The accuracy of such measurements with the oscilloscope (*delta-time measurement accuracy*) is given with 2 ps under optimal conditions [Agi13]. So even under non-optimal conditions the resolution can be assumed to be better than the rise-time of the photo-diode ($<$ 500 ps [ALP19]). Therefore, one can conclude that the tests of the delay-setting are accurate at a level of 100 ps or better. The standard deviation of these measurements is found to be $\leq$ 30 ps, further strengthening the assumption.

Therefore, the monitoring is sufficient to probe the delay-setting since its smallest possible steps are 500 ps. For both delay-lines measurements were performed in which each switch[30] was tested individually. Additionally, for the delay-line of Laser Tuebingen several further measurements were performed in which different combinations of switches have been tested. In all measurements performed, the expected delay was reached with deviations less than 200 ps, in most cases less than 100 ps. Since both delay-lines were designed identically, multi switch testing of the delay-line connected to the driver of Laser Innsbruck was omitted. During the measurements described in Chapter III and Chapter IV the PD and the oscilloscope kept being used for monitoring the setup. Therefore, proper delay-setting was always ensured.

II.2.2. Reflections

Due to the high amount of reflective optical devices used in the setup, such as the filters and the beam-splitter cube, reflections appearing several nanoseconds after the pulses are a realistic threat. As a matter of fact, about 20 ns after the pulses small[31] features appear in the oscilloscope. However, these are minor: first of all, these features are not detected by the PDP-module. Furthermore, 20 ns indicate a light path of $\approx$ 60 cm. The longest distance in the setup where major reflections could be expected is between the lasers and the filter-wheel. However, these are only 17 cm[32]. Finally, the features do not have the same shape as the initial pulses (actually, they resemble a damped vibration). Taking all this into account the most likely origin of the features visible in the oscilloscope are reflections on the cable transmitting the signal from the PD to the oscilloscope due to impedance mismatch. Therefore, the setup and measurements can be considered to be free of significant reflections.

II.2.3. Determination of the Gain

To determine the gain of the setup, single photo-electron measurements, as described in Section I.2.1, were performed. When completed, the maximum of the upsampled traces was used for reconstruction in the linear regime. Therefore, during the analysis the gain for *umax* (*ugain*) was determined. With Equation 8 the gain for *pzmax* (*pzgain*) for channel *i* can be calculated. The determined values are listed in Table II.1.

$$pzgain_{\mathrm{i}} = ugain_i \left[\frac{pzmax_{\mathrm{i}}}{umax_{\mathrm{i}}} \right] \tag{8}$$

To calculate these values, the PM-response function, derived and explained in [Bel94], is fitted onto the *umax*-values of each channel with the program *FCSPEFit*. In our setup this results in 12 output files, each containing the fitting parameters for one channel. There are seven free parameters for each fit. Therefore, the fits are not stable and the exact result depends on the starting values of these parameters. Subsequently, an error of about 0.20 is given for the gain. However, in the results presented in Chapter IV

[30] Nominally 0.5, 1, 2, 4, 8, 16 and 32 ns

[31] "'small"': $U_{\mathrm{feature}} < 0.05\, U_{\mathrm{pulse}}$

[32] With the path laser – filter-wheel – laser being 34 cm

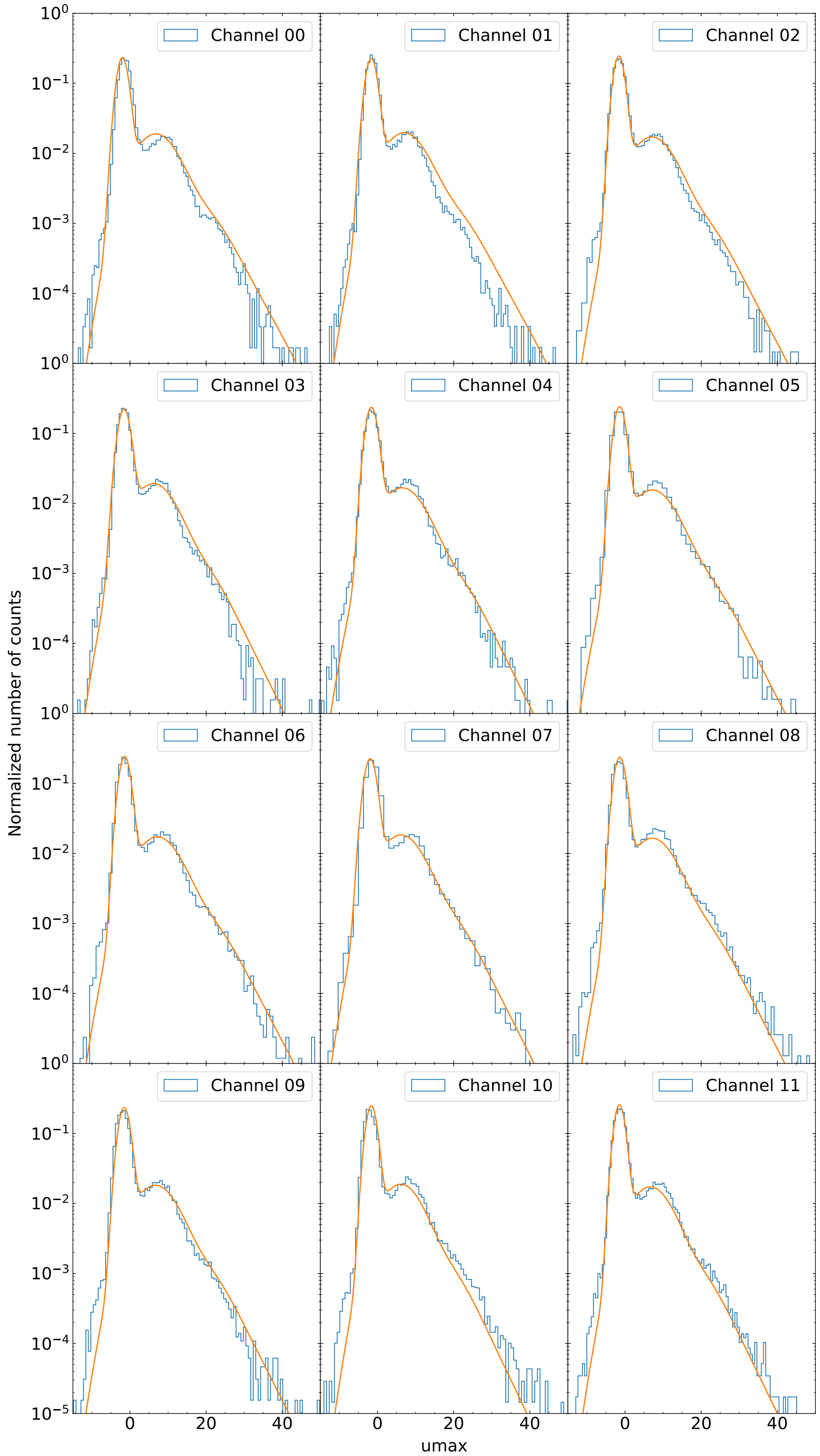

Figure II.5.: Spectra of *umax* from SPE-measurements together with the fitted PM-response function. The spectra are normalized.

Table II.1.: The table shows the gains for *umax* and *pzmax*, determined with SPE-measurements. They are valid for those PMT-voltages which are set when using "'setup_new.sh"'. According to the fitting program FCSPEFit, the error is about 0.20 for *ugain* and subsequently about 0.12 for *pzmax*. This corresponds to an error below 3%.

Channel	*ugain*	*pzgain*
0	8.4	5.1
1	8.0	4.8
2	7.9	4.8
3	7.6	4.6
4	7.6	4.6
5	8.1	4.9
6	8.5	5.2
7	8.4	5.1
8	8.5	5.1
9	8.0	4.8
10	8.6	5.3
11	8.4	5.1

mostly normalized values are considered. This means that a possible miscalculation of the gain would balance out during the evaluation.

To plot the spectra with the fitted response functions (see Figure II.5) the script *PlotSPEFitUmax.py* can be used. The plots show channel 0-11 of the FlashCam Test-Setup. The measurements were performed with Laser Tuebingen. Values below 0 can be seen on the x-axis; this is due to the relatively broad pedestal and non-perfect measurements/evaluations. However, the 1-p.e.-peak is clearly visible in all measurements. In some plots even the 2-p.e.-peak can be surmised. Therefore, the gains determined in these measurements and presented in Table II.1 are sufficiently accurate for the purpose of this thesis.

It shall be stated that the software mentioned already existed. The only contribution by the author of this thesis was to ease the handling of the script PlotSPEFitUmax.py.

II.2.4. Different Methods to Vary the Laser Intensity

To gain more freedom how to operate the experiment, it is necessary to verify that there is no difference in the system response between attenuation of the lasers via optical filters or via the laser drivers. The shape of the laser pulses might change when varying the output intensities of the lasers. In order to remove these doubts, measurements at the PDP-module are performed. Both lasers are measured individually. Initially, both are set to the highest amplitude and the filter-wheel is put in place so that the measurement can be performed in the linear regime. The intensity of the pulse is measured with the PDP-module and the PD. The same procedure is repeated with filters nominally allowing transmission of 50%, 10% and 1% of the light. For the filter with the lowest transmission rate, the filter-wheel needs to be set to a less opaque position, otherwise the pulse would not be recognizable by the PDP. The filter-wheel position for this measurement is recorded. Having finished these measurements, the filters are removed. By lowering the laser output-intensity an attempt is made to reach intensity-levels identical to those measured with the photo-diode. When the best suitable position is found, the intensity actually measured at the PD is noted and a measurement with the PDP-module is performed. For the lowest intensity the filter-wheel is reset to the position noted earlier.

The results of these measurements are displayed in Figure II.6. On the lower x-axis the relative intensity is plotted. It is defined in such a way that the maximal intensity settable at the laser-drivers is 1 and the value at which the lasers switch from lasing to non-lasing regime is 0. All ticks on the x-axis in between are interpolated linearly. On the upper x-axis the nominal optical density[33] is plotted. Using the intensity measured with the photo-diode the upper and the lower x-axis are aligned. On the y-axis, one can see the intensity measured by FlashCam. Since all measurements are performed in the linear regime, the parameter *pzmax* is used.

As stated, the filter-wheel was set to a more transparent position in order to make the measurements at the lowest intensity clearly detectable with the PDP-module. For plotting these values properly together with the others the values of *pzmax* (and, for Laser Innsbruck, of the relative intensity) had to be corrected. By performing those corrections the assumption was made that the photo-diode output is more easy affected by changes in the laser pulse-shape than FlashCam. This assumption is reasonable since the PD is very fast rising. Therefore, additional features that might appear in the pulse-shapes but would not be detected by the PD, would neither be able to affect the camera response. For Laser Innsbruck two corrections were applied, shown in Equation 9 and in Equation 10.

$$pzmax_{\mathrm{korr,1}} = pzmax_{\mathrm{meas}} \left[\frac{PD_{\mathrm{goal}}}{PD_{\mathrm{meas}}} \right] \tag{9}$$

$$pzmax_{\mathrm{korr,2}} = pzmax_{\mathrm{korr,1}} \left[\frac{PD_{\mathrm{goal}}}{PD_{\mathrm{max}}} \right] \tag{10}$$

Equation 9 is applied to shift the lowest measured value without filters on the x-axis to the lowest value with filter. This is necessary since Laser Innsbruck is not sufficiently fine-tunable to reach the relative intensity given by the od=2.0-filter. $pzmax_{\mathrm{meas}}$ is the actually measured value for pzmax (in the measurement with lowest intensity set), PD_{meas} is the corresponding output of the photo-diode. PD_{goal} is the output of the photo-diode measured at full intensity but with the od=2.0-filter. Finally, $pzmax_{\mathrm{korr,1}}$ is the pzmax-value that would be expected if the laser intensity could be set to a sufficiently low level.

Laser Tuebingen can be tuned more accurately. Therefore, the first correction step is not necessary and it can be identified $pzmax_{\mathrm{meas}} \equiv pzmax_{\mathrm{korr,1}}$. PD_{goal} is still the output-value of the photo-diode for the examined measurement. For Laser Innsbruck, PD_{goal} is for both measurements equal (following the first correction); for Laser Tuebingen they are slightly different ($\pm 10\%$). PD_{max} is the photo-diode output of the maximum intensity[34]. Finally, $pzmax_{\mathrm{korr,2}}$ is the corrected value; plotted in Figure II.6.

The measurements were, as the plots indicate, successful. Identical values of the PD-output lead to identical *pzmax*-values. Therefore, a possible change of the pulse-shape has no impact different from an optical filter. It can be concluded that it is possible to both attenuate the lasers with the exchangeable optical filters or via attenuation of the laser pulses themselves.

[33] See Footnote21 in SectionII.1.

[34] Full intensity from the laser-driver without use of a filter

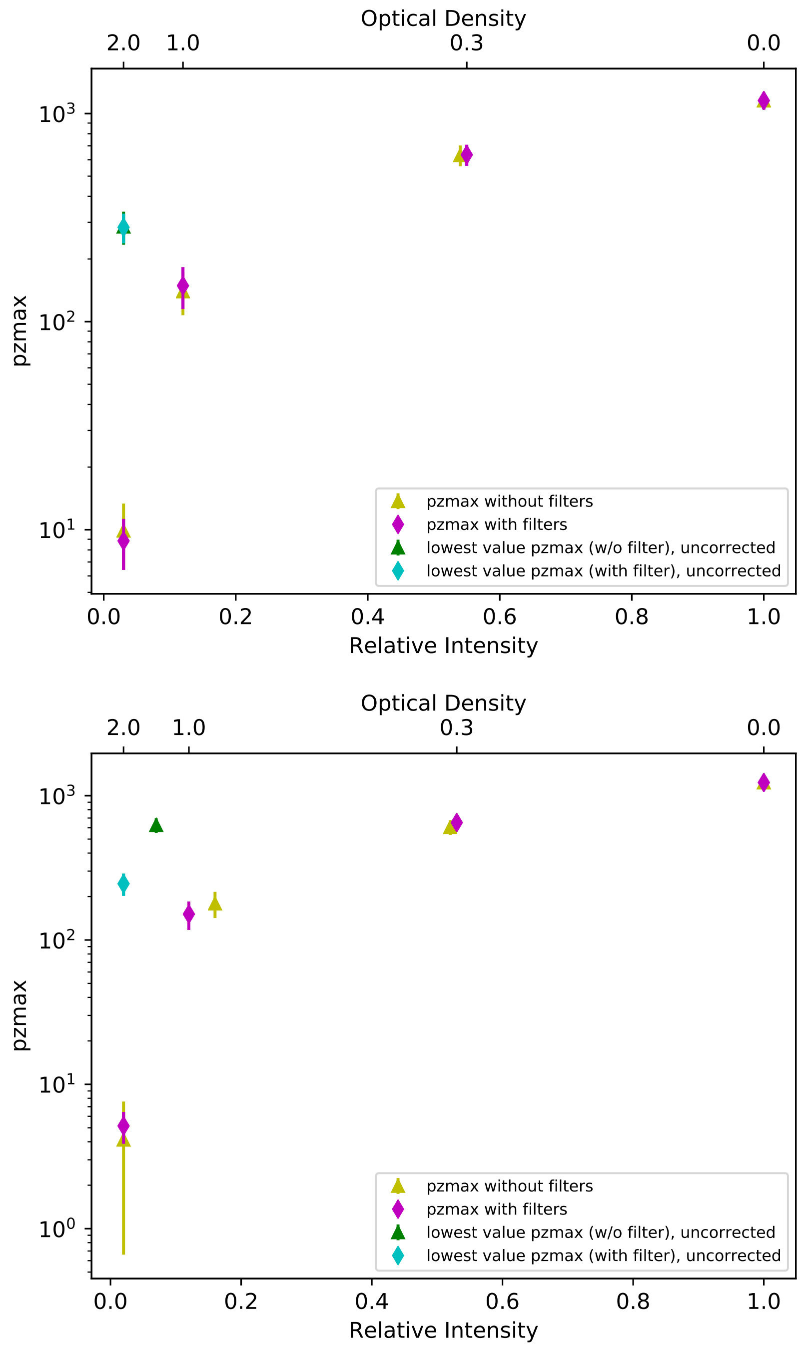

Figure II.6.: Measurements with and without additional filters but at similar relative intensities. Top: Results for Laser Tuebingen. Bottom: Results for Laser Innsbruck. Since the driver for Laser Innsbruck is not as finely tunable as the other, the values are scattered along both axis. The green and cyan colored values are measured with a more transparent filter-wheel setting than the others. The lowest values in yellow and purple are reconstructed using data collected by the photo-diode. The error bars are given by the standard deviation of the measurements (each data-point is an average over all channels and 30 000 measurements) and gaussian error propagation, respectively. If only one data point is visible, the corresponding one is hidden behind.

III. Measurements

The goal of this experiment is to estimate experimentally the response of FlashCam on realistic light pulses as they appear in gamma-ray induced air-showers. These pulses are simulated by two pulsed lasers which are fired with a variable temporal delay Δt. For larger delays, the response on two separated laser light pulses can be determined. To achieve this, different *measurement scenarios* have been developed. A measurement scenario is a specific setting of the two laser intensities relative to each other. Each scenario is realized in the linear and in the non-linear regime of the camera. Further, one scenario specifically probes the transition regime. With the NSB-LED installed in the darkbox different levels of background illumination are applied to all measurement scenarios (for all regimes).

The settings and a detailed description on how the measurements were performed is given in Section III.1. Section III.2 is dedicated to the analysis procedure of the data recorded and the uncertainties. Finally, in Section III.3 the expectations for the results of the measurements presented in Chapter IV are given.

III.1. Measurement Procedure

Table III.1.: Overview-table for the different measurement-scenarios.

Scenario	Regime	Description
od00	linear, transition & non-linear	both lasers at same amplitude
od03	linear & non-linear	one laser attenuated by 50%
od10	linear & non-linear	one laser attenuated by 90%

Three measurement scenarios are performed. The differences in the laser intensities relative to each other are reached by placing filters with different optical densities in front of the lasers[35]. In the simplest case both lasers are at the same amplitude and therefore, no filter is needed. Since this corresponds to an optical density of 0, this measurement scenario is labeled as *od00*. For the two other scenarios filters with optical density 0.3 and 1.0 are used[36] individually, leading to relative intensities of 2:1 and 10:1. These measurement scenarios will be referred to as *od03* and *od10*. An overview over all measurement scenarios realized can be found in Table III.1

For each delay to be measured[37] a measurement of 30 000 samples is recorded. After first evaluations additional steps are added around delays with large derivatives of the measured quantities. For measurement scenarios with filters, two cases must be taken into account: one in which the first firing laser is attenuated and one in which the second

[35] At the position labeled with *ND-Filter (opt.)* in the setup (FigureII.2)

[36] Following Footnote 21, this would lead to transmission rates of 50% and 10%, respectively. However, the actual optical density in the wavelength regime of the lasers is lower than that (see Figure B.3 and Figure B.4).

[37] 0 ns to 40 ns for measurements in the linear regime and up to 80 ns in the non-linear and the transition regime with step widths between 1 ns and 5 ns.

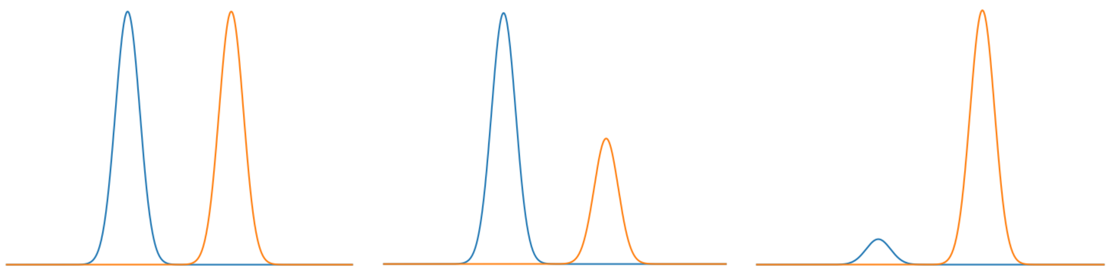

(a) od00: the front and the rear pulse have the same amplitude

(b) od03_last: the rear pulse has half the amplitude of the front pulse

(c) od10_first: the amplitude of the front pulse is 1/10 of the rear pulse amplitude

Figure III.1.: Examples for different laser-pulse scenarios. Pulse widths and amplitudes are not to scale.

firing laser is attenuated.[38] Each delay setting needs to be measured for both cases. To distinguish them, the measurements are marked as *first* or *last* when the filter stands in front of the first or the last firing laser. However, in the od00 scenario *first* and *last* measurements would lead to the same results since there is no filter to place in front of any of the lasers. Therefore, there is no labeling of this kind. Further, in the respective plots which display the measured quantities against the delay of the particular measurement the plots from the od00 scenario are mirrored at the $\Delta t = 0\,\text{ns}$ axis. Examples of the different scenarios are given in Figure III.1.

During analysis all measurements of the same scenario, the same regime and with the same NSB are processed together as one *series of measurements*. They are evaluated with the same parameters and the plots show the whole series.

In general, the command for the FlashCam camera server software to perform a measurement is

./efbprun ./test-fc250b -ei enp1s0 -et efb0 -a 21 -athr 0 -athr 100,23,1 -bl 200 -sd 0 -es 320 -me EVENTS -o FILENAME

Here, *./efbprun ./test-fc250b -ei enp1s0 -et efb0 -a 21* starts the FlashCam software, defines the Ethernet interface (*-ei*), the Ethernet type (*-et*) and the address of the FADC-module (*-a*). Further, *-athr 0 -athr 100,23,1* initially disables the internal trigger for all channels, before setting the trigger level to 100 LSB for one channel, starting from channel 23 (⇔ enables triggering on channel 23 only)[39]. Further, *-bl 200* sets the baseline to the arbitrary value of 200 LSB. *-sd 0 -es 320* defines the number of readout samples per event to be 320 (corresponding to 1280 ns readout time) and a storage delay of 0 samples. The storage delay offers the possibility to read out samples which occurred before the trigger. Since in our setup the measurement signals arrive in the camera more than 1000 ns (250 samples) after the trigger signal, storage delay is not necessary. Finally, the parameter *-me* defines the number of events to be recorded and *-o* the path to save the output-traces as a binary file.

As already mentioned, all measurement scenarios were performed with night-sky background, too. NSB acts on a Cherenkov-telescope camera by providing a constant flux of photons and is inevitable in observations. It can be regarded as an additional

[38] It is of relevance to distinguish these two cases, since effects such as pile-up might behave different, depending on which pulse is stronger. See also Section III.3.

[39] In operational mode FlashCam will trigger as described in Section I.2.2

(but not perfectly constant) baseline that is added to the electronic baseline set with the camera software.

For NSB-measurements the LED is turned on to illuminate the interior of the darkbox at levels[40] of 300 MHz and 1500 MHz corresponding to a barely illuminated and bright night-sky. For one series of measurements (od00 in transition regime) NSB=3 MHz is also measured. This is because from earlier experiences with PMTs, a gain-drop between no background at all and this unrealistically low background can be expected. This should lead to a comparably large difference in the number of pe_{rec} between the two cases. In preliminary NSB-measurements of all scenarios and regimes such a step was already found between the series with the NSB-LED being switched off and the series with 300 MHz illumination.

Before turning on the LED the baseline has to be set once at the desired level (usually 200 LSB). If the baseline was set after turning on the LED, the LED would cause some noise around the set baseline. However, the focus of LSB-measurements is on the baseline-shift due to different LSB-levels. This baseline-shift would be blanked out by a resetting of the baseline when the LED is already turned on, which therefore must be avoided. For this reason the option *bl* must be removed from the initializing command and the baseline must be set once at the beginning of the measurements.

Switching between the regimes means the intensity of the laser pulses reaching the PDP-module must be changed. Since it is a challenging task to adjust the two different laser systems to the same intensity, it is best to not change them. Instead, switching between the regimes can be achieved by rotating the filter wheel to a more/less transparent position, depending on the desired change in the intensity.

III.2. Analysis

The fc-utils programs are a collection of software tools used for analyzing the FlashCam calibration measurements. When the work for this thesis started, *FCTraceAnalyser* was the program used to extract parameters from FlashCam measurement data. During the time the present thesis was written it has been replaced by *FCEventReconstructor*. The new program is faster and returns less parameters. Therefore, the analysis of the measurements also switched from FCTraceAnalyser to FCEventReconstructor.

Since FCEventReconstructor is the more recent program, all the information given here refers to it. It processes each measurement by executing the steps of digital signal processing as described in Section I.2.3 for each individual trace. To not lose any information during evaluation, no search window is used and therefore, always the whole trace is evaluated. The configuration values that were determined during validation (see Section II.2.3 and used for the analysis can be found in Appendix C. A script was written that allows for processing a directory with measurement data, typically containing a whole series of measurements at once.

As its predecessor, FCEventReconstructor returns multiple statistical values for each trace. However, in the context of this thesis mostly needed are $pzmax$, A_{1200}, w_{d} and pe_{rec}, being measures for the reconstructed intensity. In the software, these parameters are labeled as $pzmax$, $ufwsumbs1200$, $dwidth$ and $perec$. In some cases (especially in the overlap zones of the regimes) it is of interest to know the number of photo-electrons reconstructed with the individual methods instead of the returned pe_{rec} only. These are included in the output-files of FCEventReconstructor, too. The definition of these values and how they are calculated is explained in Section I.2.3. For further processing a series

[40]The NSB level is given as a frequency, being the count-rate of NSB photons per pixel.

of scripts was written which reduce the output-data from FCEventReconstructor step by step. All these scripts are written so they process a whole series of measurements inside a directory at once.

The values of one parameter are read out by *EvtsRec2ParameterDir.py*. For each channel and measurement all values of the given parameter are written into an individual file. The twelve files for each measurement and parameter are saved in an individual directory.

The next step in the data reduction chain is the script *ParameterStats.py*. It creates a statistics file in which the average, the median and the standard deviation for each parameter and each channel are displayed. At the end of these statistics-files either the average over all averages or over all medians is displayed. This value is considered to be the result of a measurement and shall be referred to as a *data point*. Using the average of the medians to define a data point is a useful option if in all channels, a significant number of values is too high due to miscalculation.[41]

Finally, the data points of one series of measurements are condensed into one file with the script *StatsEvaluator.py*. Its output file includes the data points of all parameters extracted previously, ordered by the Δt of the corresponding measurement.[42] Additionally, the data points are not only available as absolute values but also normalized. For that, the values of the data points are divided by the value of the data point of the corresponding parameter at $\Delta t = 0\,\mathrm{ns}$.

To further automatize the evaluation of a series of measurements, another script was written. It calls the scripts mentioned previously and extracts all necessary parameters at once (*Masterscript.py*).

To visualize the results plots were generated. They display Δt on the x-axis and the normalized value of the data points from the different parameters on the y-axis.[43]

The uncertainty of the value of each data point is determined by applying statistics. To better understand the method it shall be summarized how the values are calculated. For each measurement the average is calculated for each channel[44]. Afterwards, the average over all channels is calculated and taken as the value of that data point. In all measurements presented in Chapter IV there were twelve channels used and each channel recorded 30 000 events. To determine a uncertainty for a measurement the highest uncertainty of the individual channels is used. This ensures that the given uncertainty is not too low. It is given as the standard deviation of the mean, being

$$\sigma_\mathrm{m} = \frac{\sigma}{\sqrt{n}} \tag{11}$$

with σ being the largest standard deviation of a channel in this measurement and $n = 30\,000$ being the number of events. Since only normalized values are plotted it is sufficient to only consider the normalized σ_m, again being the absolute values of σ_m divided by the absolute value of the data point at this $\Delta t = 0$. It turns out that for all measurements[45] $\sigma_\mathrm{m} < 1\%$.[46] Therefore, the plots displayed in Chapter IV will not include error bars. In the cases in which the evaluation worked properly they would be invisible, in all the other cases they would make the plots unreadable.

[41] In Chapter IV, examples are presented.

[42] *first*-measurements are defined as $\Delta t < 0$ and *last*-measurements as $\Delta t > 0$.

[43] In few cases the absolute number of pe_rec is plotted

[44] In case of default settings. In special cases the median is used.

[45] Except for those with a bug in the evaluation. However, in those cases the uncertainty would be higher than any value realistic for FlashCam. This strengthens the point that there is a bug in these evaluations.

[46] In most cases $\sigma_\mathrm{m} < 0.5\%$

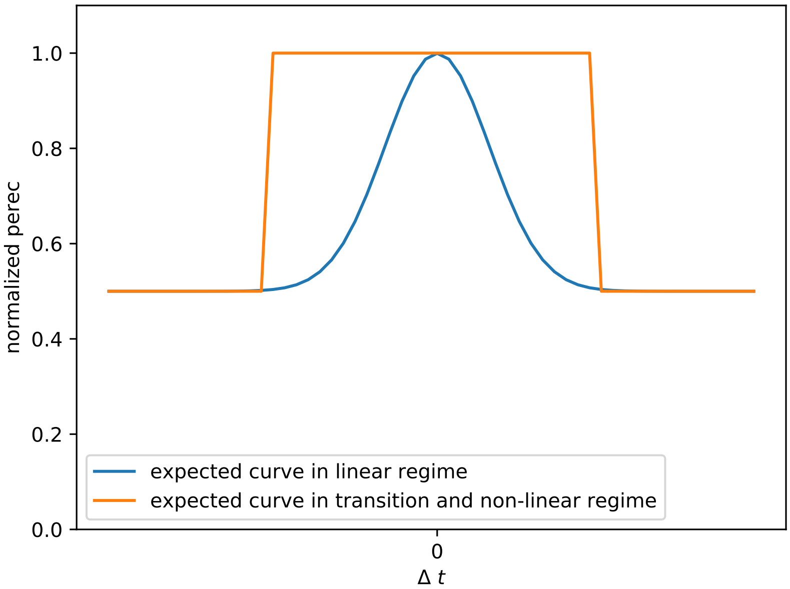

Figure III.2.: Expected shapes of the curves in the od00 scenario. The values at the end of the plateau of the curve for the transition and the non-linear regime are expected to drop less abruptly. In the transition regime, the plateau in the center should be less broad than in the non-linear regime. The x-axis is not to scale (except $\Delta t = 0$).

III.3. Expectations

There are clear expectations on how the plots produced by the measurements and with the analysis procedure explained in the two previous sections should look like. In all regimes the measurements have been normalized so that at $\Delta t = 0\,\text{ns}$ the normalized values of all parameters are defined as 1.[47] Especially for the reconstructed intensity in units of pe_{rec} one expects the normalized data points at the left and the right edges of the plots to reach a limit, determined by the scenario: in the od00 scenario it is 0.5, in the od03 scenario it is 0.66 and in the od10 scenario it is 0.9. The limit will be reached when both pulses can be fully separated and the raw trace returns to the baseline in between. Then, only the stronger pulse should be considered in reconstruction since both pulses are recorded. Therefore, the limits are given by the fraction of the total intensity that is in the stronger pulse of each scenario.

Especially in the od00 scenario, deviations from the limit have to be expected, since the intensities of the two lasers have to be equalized by looking at the raw traces "'by eye"'. In this scenario deviations should only create values larger than the limit of 0.5, since the larger pulse should always be reconstructed. In the other scenarios values smaller than the limit may appear, depending on which laser is attenuated in each case.[48] Further, it has to be considered that the filters do not match their nominal optical densities[49] in the wavelength regime of the lasers and therefore, the actual limits vary by a

[47]Except the case that a parameter is not calculated, such as for w_{d} in linear regime in the latest version of FCEventReconstructor.

[48]Since the intensities of the lasers are not equal the pulse might be below the limit, if the stronger laser is attenuated.

[49]See Figure B.3 and Figure B.4 in the appendix.

few percent.

The shape of the curve between these fixed points at $\Delta t = 0$ ns and Δt being maximal depends on the regime rather than on the scenario. In the linear regime a bell-shaped curve is expected as shown in Figure III.2: Already at very small Δt ($\gtrsim 1$ ns) the maximum of the pz-corrected trace is lower than at $\Delta t = 0$ ns since the two traces do not totally overlap anymore. Therefore, for every $\Delta t \neq 0$ the reconstructed intensity should be smaller than 1.[50] The value will decrease, until both pulses are fully separated. It has then reached the limit and stays constant. Following preliminary results from A. Gadola from the UZH Zürich the limit should be reached at $10\,\text{ns} \leq \Delta t \leq 15\,\text{ns}$ in the linear regime.

In the non-linear regime the (normalized) values of pe_{rec} at the left and the right edge should match those in the linear regime, as indicated in Figure III.2. However, no bell-shape is expected: just as the *pzmax* in the linear regime, the w_{d} in the non-linear regime should just be added up to each other. As long as the pulses can not be separated, it is expected that w_{d} returns always the same value since the traces have a mostly rectangular shape (see Figure I.10). However, at specific Δt there should be a prompt transition from overlapping to not overlapping such that only the stronger pulse is considered. In the plots of the normalized reconstructed intensities, this should lead to a plateau of value 1 as long as the pulses overlap. When Δt becomes sufficiently large and they can be separated, the reconstructed intensity should decrease extremely fast to the limit that is determined by the regime.

In Figure III.2 this shape of the plots is indicated by a Heaviside function. Because there is some jitter the values will not drop that abruptly in actual measurements. Since both pulses are in the non-linear regime, the fast decrease is not expected to happen at $\Delta t \lesssim 10$ ns.

The data of the normalized reconstructed intensity in units of pe_{rec} over time in the transition regime is expected to qualitatively produce the same plots as those in the non-linear regime. However, the plateau should be less broad, simply due to the fact that the traces last for a shorter time. The reason for the plateau is technically the same: as long as the two traces (above 1200 LSB[51]) are inseparable, the normalized reconstructed intensity should be 1. When they can be separated the value should drop to the limit. Again, time jitter is the most important reason that the corners of the curve in Figure III.2 will be smoothed out a bit.

There is another feature concerning the non-linear regime that should be discussed: In the od03 and od10 scenario the plateau will reach to larger Δt for $\Delta t > 0$ ns than for $\Delta t < 0$ ns. This is because in the case > 0 ns, the attenuated pulse comes (temporally) after the non-attenuated pulse. As described in Section I.2.3, the intensity of a pulse in the non-linear regime is indicated by its duration. Therefore, the non-attenuated pulse lasts longer than the attenuated one. Consequently, it requires larger Δt to separate the two pulses if the non-attenuated is fired first rather than the attenuated one.

[50] Since the reconstruction in the linear regime is linear, the curves of pe_{rec} and *pzmax* should show the same features. However, in the other regimes pe_{rec} will not follow the relevant parameters, being A_{1200} and w_{d}.

[51] 1200 LSB, since A_{1200} is used for reconstruction in the transition regime

IV. Results

In the first section of this chapter the results obtained with previous versions of the reconstruction program are explained. The results obtained with the latest version of this program are presented in Section IV.2, where also remaining issues are discussed. Different results for the same scenario and regime are due to reconstruction only. The measurements themselves remain unchanged. Finally, the chapter concludes with a discussion of necessary changes that have to be implemented in the software.

IV.1. Results Leading to Improvements in Analysis Software

While the experiment was being prepared and performed the main analysis tool changed from FCTraceAnalyser towards FCEventReconstructor. The most important difference between these two programs is that FCEventReconstructor supports reconstruction of the number of p.e., which serve as a measure of the intensity and FCTraceAnalyser does not.

Further, the experiment described is the first of its kind (firing two laser pulses on FlashCam with a temporal delay) that is fully evaluated.[52] Therefore, these measurements are of use not only to obtain a better understanding of the camera response on hardware level but also to test and improve the newly written reconstruction software and find possible bugs in it, as well as in the analysis algorithms in general.

For comparison, this section initially shows the values obtained with the last updated version of FCTraceAnalyser. Then the evaluation of the measurements with the first version of FCEventReconstructor is presented. Information on the parameters and the reconstruction of the number of p.e. can be found in Section I.2.3.

IV.1.1. FCTraceAnalyser, version of October 9, 2019

Since FCTraceAnalyser does not allow reconstruction of the number of p.e. only plots of the regime-dependent parameters are shown. This means that the expected shapes of the plots (see Section III.3) should appear, however, the limits introduced will only be valid for $pzmax$ and not for A_{1200} or w_d.[53] Figure IV.1 shows the normalized value of the pole-zero corrected maximum of the trace of different measurement scenarios in the linear regime. In Figure IV.2 the normalized values of A_{1200} in od00 scenario in the transition regime are plotted. Finally, in Figure IV.3 the normalized w_d of several measurements in the non-linear regime is displayed.

For the curve in the linear regime it is obvious that the relevant parameter is measured correctly. The limits are 0.53 for the od00 scenario (red), 0.67 on the left ($\Delta t < 0\,\mathrm{ns}$) and 0.64 on the right side ($\Delta t > 0\,\mathrm{ns}$) for the od03 scenario (blue) and 0.86 (left), respectively 0.89 (right) for the od10 scenario (green). The deviations from the theoretically expected values can be traced back to two issues already mentioned in Section III.3: first, it is

[52] The analysis of the measurements by A. Gadola mentioned above never exceeded the "'preliminary"' stage.

[53] This is, because in the transition regime and the non-linear regime the relevant parameters (A_{1200} and w_d) are not proportional to pe_rec.

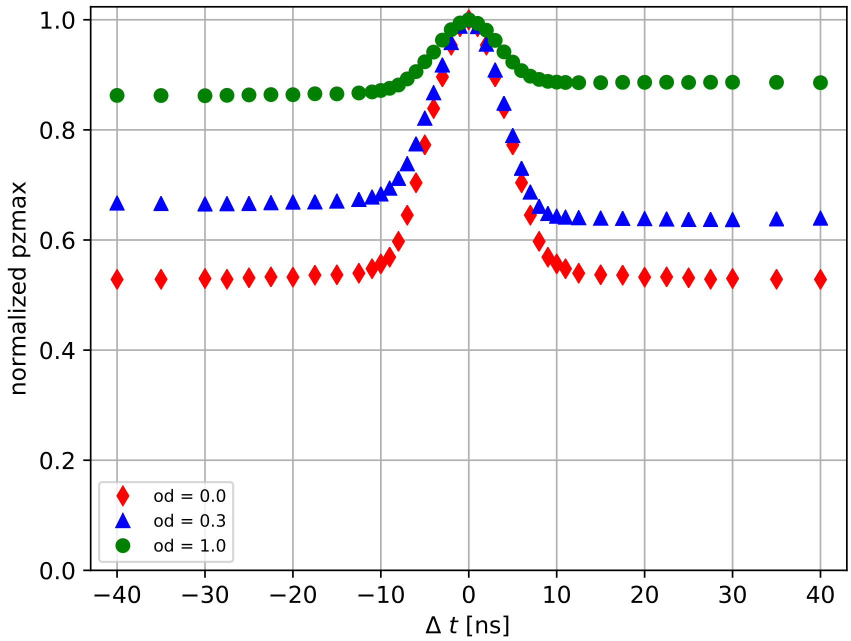

Figure IV.1.: Normalized pole-zero corrected maximum of the three scenarios in the linear regime. Analysis was performed with FCTraceAnalyser in the version of October 9, 2019. The curves have the expected shape.

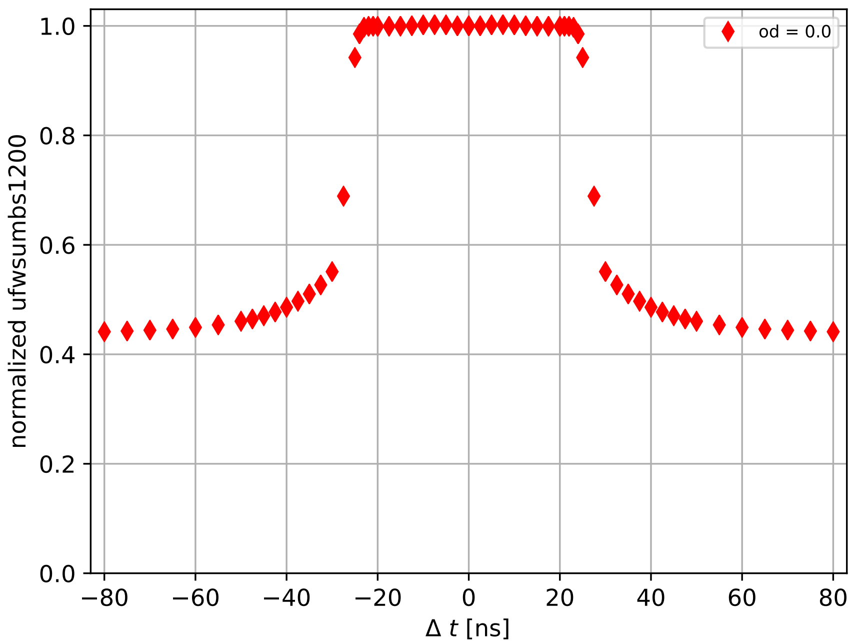

Figure IV.2.: Normalized area over 1200 LSB (A_{1200}) for the od00 scenario in the transition regime. Analysis was performed with FCTraceAnalyser in the version of October 9, 2019. The curve has the expected shape.

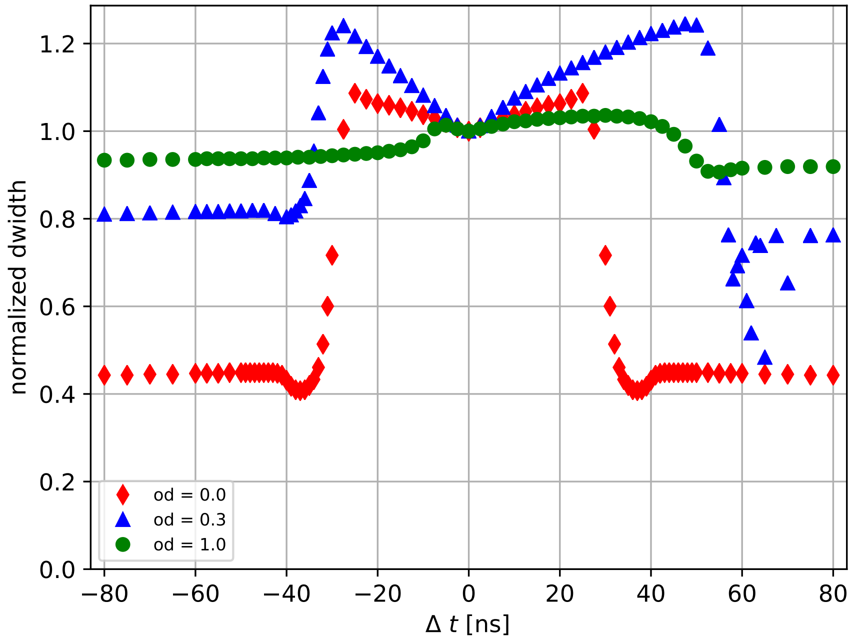

Figure IV.3.: Normalized w_{d} of the three scenarios in the non-linear regime. Analysis was performed with FCTraceAnalyser in the version of October 9, 2019. The curves show several unexpected features, the most drastic being values larger than 1.

very challenging to align the two different lasers intensities perfectly. Second, the filters do not show their nominal optical density over all wavelengths, as displayed in the appendix (Figures B.3 and B.4). The limit of *pzmax* is reached at the expected Δt, being between 12.5 ns and 11 ns.

In the transition regime the data behave as expected. A plateau of A_{1200} being at 1 and exceeding up to little over $\Delta t = 20$ ns is followed by a fast decrease. The curve finally shrinks to the limit 0.44. Since the single pulses in this scenario are not clipping and the reconstruction algorithm uses an offset (see Equation 5). This roughly seems to be fine. However, only reconstruction of pe_{rec} as possible with FCEventReconstructor can show if it actually is.

In the non-linear regime, the normalized curves for w_{d} show several unexpected features. First of all, there is no plateau as found in transition regime. Indeed, the values increase linearly between $\Delta t = 0$ ns and the steep decrease. This stays the same for FCEventReconstructor and is discussed in Section IV.2. The limits found for these series of measurements are 0.44 in the od00 scenario, 0.81 (left) and 0.76 (right) in the od03 scenario and 0.92 (left), respectively 0.93 (right) in the od10 scenario. Without knowledge of the calibration constants used in the exponential reconstruction function for the non-linear regime (Equation 4) it cannot be trivially stated if these limits are reasonable or not.

The next feature to be looked at is where the curves decrease steeply. One finds that this decrease happens at lower Δt for the od00 scenario than for the other scenarios. This is due to the fact that this scenario is measured with a lower total intensity than

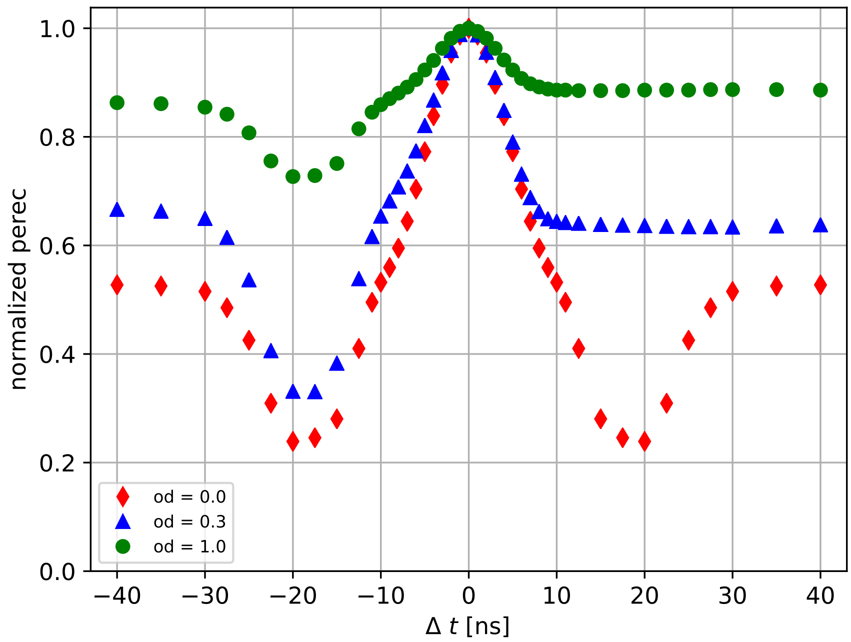

Figure IV.4.: Normalized pe_{rec} of the three scenarios in linear regime, analyzed with FCEventReconstructor of November 6, 2019. The curves show a relict caused by the reconstruction algorithm around $\Delta t = 16$ ns. The double-dip of the o.d.=0.0-curve (red) is due to the mirroring at $\Delta t = 0$ (see Section III.1)

the od03 scenario an the od10 scenario.[54] For the two other scenarios the initial, non-attenuated pulses have the same amplitude and the steep decrease happens at lower Δt for od10 than for od03: the attenuated pulse in scenario od03 is stronger and therefore lasts longer. Finally, one finds that the decrease happens on the right side at much larger Δt than on the left side. This is because the non-attenuated laser (firing first) causes a longer lasting trace than the attenuated one. Therefore, larger Δt are necessary to separate the pulses.

Finally, after the steep decrease of the curves, there is another unexpected feature: a kind of undershoot, especially in the blue (od03-scenario) curve around $\Delta t = 60$ ns. For this, no explanation was found before the code became outdated. However, using FCEventReconstructor this feature has disappeared.

IV.1.2. FCEventReconstructor, version of November 6, 2019

As successor of FCTraceAnalyser, FCEventReconstructor includes p.e.-reconstruction. As already mentioned, this parameter is preferred as the measure for the reconstructed intensity. The output files include the reconstructed number of p.e. for all regimes individually, as well as a final value for pe_{rec}, calculated as defined in Section I.2.3. Figure IV.4 shows the normalized pe_{rec} for the three scenarios measured in linear regime. In Figure IV.5 pe_{rec} is displayed for the od00-scenario measured in transition regime. The reconstructed number of p.e. as calculated with the algorithms for the different regimes is shown in Figure IV.6. Finally, the parameter w_{d} for the measurements in non-linear

[54] This is because at the time the measurements were performed there was no reliable reconstruction of p.e. values larger than 1600.

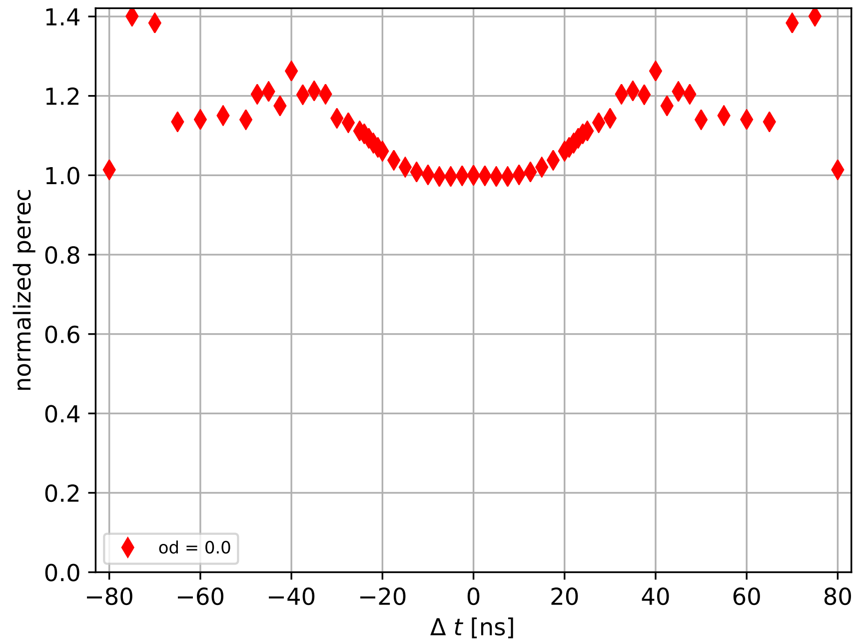

Figure IV.5.: Normalized reconstructed number of p.e. for the od00 scenario in transition regime, analyzed with FCEventReconstructor of November 6, 2019. The poor reconstruction is caused by a bug in determining the correct regime.

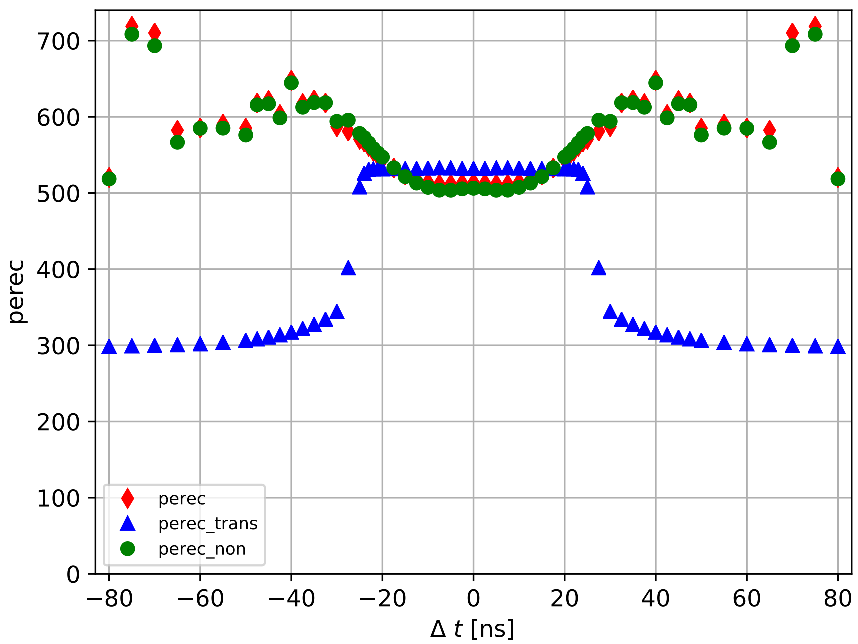

Figure IV.6.: Total reconstructed number of p.e. with reconstruction methods of all regimes for the od00 scenario in transition regime analyzed with FCEvent-Reconstructor of November 6, 2019. One clearly sees that the curve for pe_{rec}, which should follow the curve of $pe_{\text{rec,trans}}$, mostly follows the values of $pe_{\text{rec,non}}$.

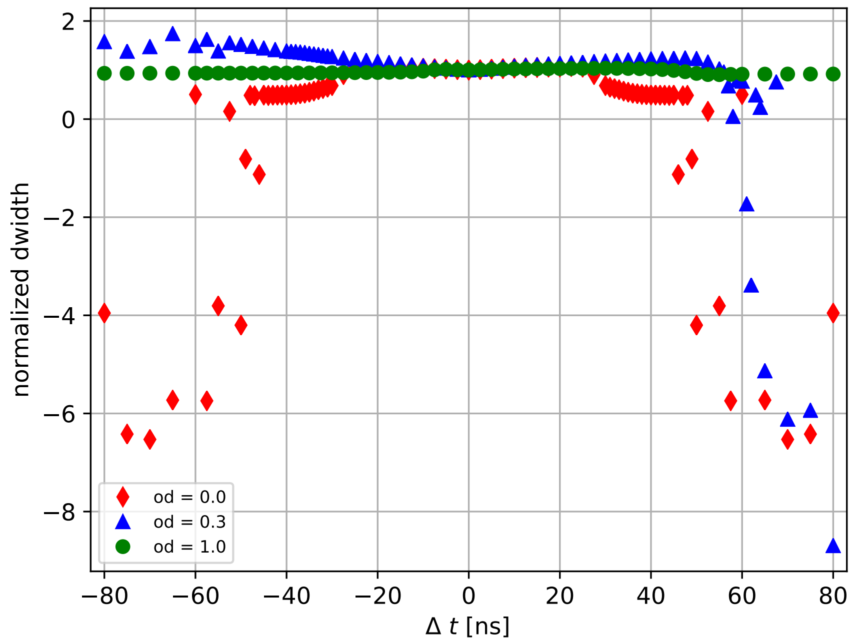

Figure IV.7.: Normalized w_d for the different scenarios in non-linear regime analyzed with FCEventReconstructor of November 6, 2019. Especially the values below 0 and those near to 2 (od03, left side) are pointing out bugs in the software.

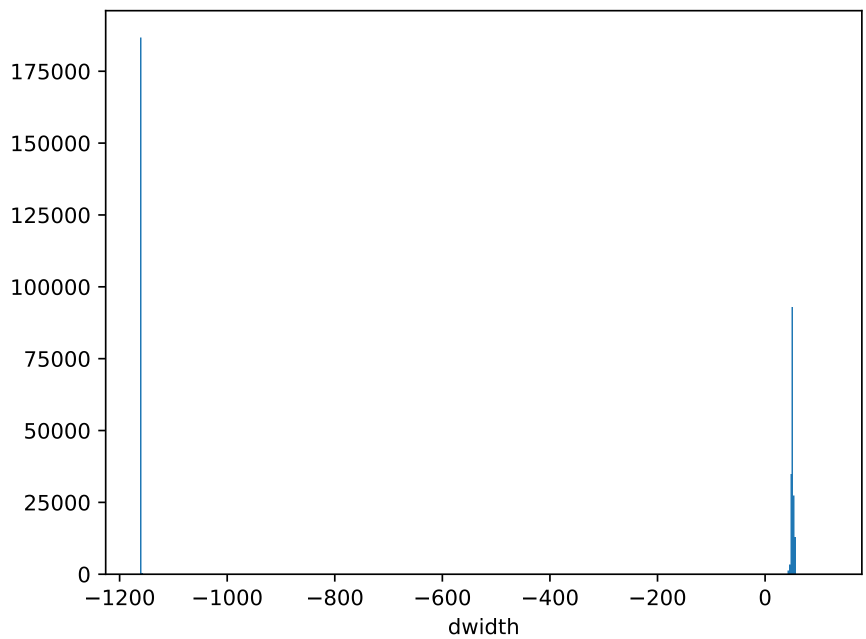

Figure IV.8.: Histogram of w_d in od03 scenario in non-linear regime at $\Delta t = 80$ ns analyzed with FCEventReconstructor of November 6, 2019, given in nanoseconds. About half of the measurements return an impossible value (-1160), due to a bug.

regime is plotted in Figure IV.7. For a better understanding of the issues in the non-linear regime a histogram of w_d in the od03 scenario at $\Delta t = 80\,\mathrm{ns}$ is displayed in Figure IV.8.

It is intended to calculate the parameters *pzmax*, A_{1200} and w_d in the same way as FCTraceAnalyser does. For *pzmax* this works out perfectly. The plot is not distinguishable from Figure IV.1 and the absolute values are the same, too. However, in the calculation of pe_rec in linear regime (Figure IV.4) an initially unexpected dip appears around $\Delta t \approx 20\,\mathrm{ns}$. This is due to the calculation algorithm of $pe_\mathrm{rec,lin}$. The background value *pzbgmax* is determined as the highest value of the pole-zero corrected trace between 16 ns and 20 ns before the global maximum of the pole-zero corrected trace (see also Section I.2.3). If $20\,\mathrm{ns} \leq \Delta t \leq 16\,\mathrm{ns}$, there will be a peak in the range where the background is determined. This leads to the background estimation being too high and therefore to the reconstructed intensity in units of pe_rec being too low at this Δt, although the normalized values for *pzmax* are fine.

At the edges of the series of measurements the normalized intensity in units of p.e. is 0.53 in the od00 scenario, 0.66 at the left edge and 0.64 at the right edge of the od03 scenario and 0.86 (left) and 0.89 (right) in the od10 scenario. Therefore, reconstruction of the intensity works properly within the unavoidable systematic uncertainties and except for $\Delta t \approx 20\,\mathrm{ns}$. In the discussion (Section IV.3) it is stated why the reconstruction in the linear regime is considered to be sufficient and how it could be further improved.

Also for A_{1200}, the calculation works well and the values are the same as those calculated with FCTraceAnalyser. However, as Figure IV.5 shows, the reconstruction of the intensity in units of p.e. did not succeed. First and most importantly, the value of pe_rec which is ultimately displayed is not mainly based on $pe_\mathrm{rec,trans}$, but on $pe_\mathrm{rec,non}$.[55] However, the pulses are too weak for reconstruction with the algorithm for the non-linear regime.[56] This happens anyway, because in the initial version of FCEventReconstructor the calculation for w_d did not work properly (this is discussed in the paragraph about the non-linear regime). Further, no non-linear threshold was implemented to avoid the reconstruction of the non-linear regime to be applied for w_d which are too low. In addition, the formation of the weighted average does not work as intended in this version of the program. This can be seen as an example for the values at $\Delta t = 70\,\mathrm{ns}$ in Figure IV.6: the value of pe_rec is higher than any of the values forming it, a result that cannot hold true.

In consequence of these bugs the limits and thresholds for the three regimes described in Section I.2.3 are introduced. Therefore, the second version of FCEventReconstructor is able to avoid most of these problems as the next section shows.

In the non-linear regime the attempt to calculate w_d as in FCTraceAnalyser failed, as Figure IV.7 shows. In the od00 scenario, normalized values at $|\Delta t|$ clearly above $> 40\,\mathrm{ns}$ can be negative, even below -6. In the od03 scenario, normalized values at negative Δt do not drop as expected and seen in Figure IV.3. Instead, they increase up to 1.6. For positive Δt they drop as the data points from the od00 scenario and reach values below -8. Only the data points in the od10 scenario seem to follow the calculations of FCTraceAnalyser.

In Section IV.2 the appearance of normalized values larger than 1 is discussed, which had been observed by both reconstruction programs. However, values below 0 should be impossible. Therefore, one data point is examined in more detail, being $\Delta t = 80\,\mathrm{ns}$ in the od03 scenario. This point is chosen since it shows the value of -8.70, the most extreme one observed. Its histogram, displayed in Figure IV.8, shows two sharp values of which the average is formed. The expected value is around 50 ns, while the large peak

[55] See Figure IV.6

[56] Especially when the two pulses are separated at $\Delta t > 20\,\mathrm{ns}$, see Figure IV.2.

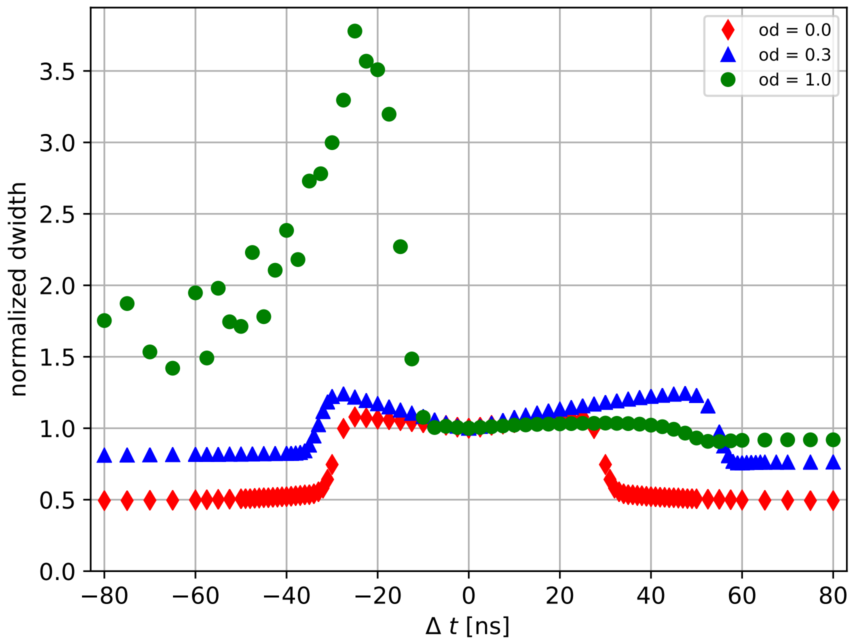

Figure IV.9.: Averaged w_d for the different scenarios in the non-linear regime analyzed with FCEventReconstructor of November 11, 2019. The curves for od00 and od03 follow the expected shape. However, the data points for od10 are obviously not calculated correctly for $\Delta t < 0\,\mathrm{ns}$.

on the left is at -1160 ns. This affects the average of the measurement and therefore the data point, leading to a impossible w_d (-579.2 ns) and subsequently to a very negative normalized value in the plot. Since about half of the values are contained in the negative bin, the use of the median would also be unstable. However, the second version of FCEventReconstructor mostly fixes this issue as Section IV.2 shows.

IV.2. Results with the Latest Software Version

IV.2.1. Improvements with respect to the previous version

The second version of FCEventReconstructor fixes the major problems described above. Since the reconstruction of the intensity in the linear regime was already fine in the previous version no changes are made in this regime. Subsequently, this section only concentrates on the transition regime and the non-linear regime. The most significant errors in the reconstruction of the intensity in units of pe_rec in the transition regime in the previous version of FCEventReconstructor are due to the missing non-linear threshold and are therefore related to the non-linear regime. In consequence, in this section the evaluation of the measurements in the non-linear regime is presented and explained before the evaluation of the transition regime.

Figure IV.9 shows the behavior of the reconstructed intensity in units of w_d in the non-linear regime in average. In Figure IV.10, the median data points of these scenarios are displayed and Figure IV.11 shows the median pe_rec in the non-linear regime. To better understand the results presented the differentiated traces of an event in the od03 scenario in the non-linear regime at $\Delta t = 0\,\mathrm{ns}$ and at $\Delta t = -30\,\mathrm{ns}$ are shown in Figure IV.12

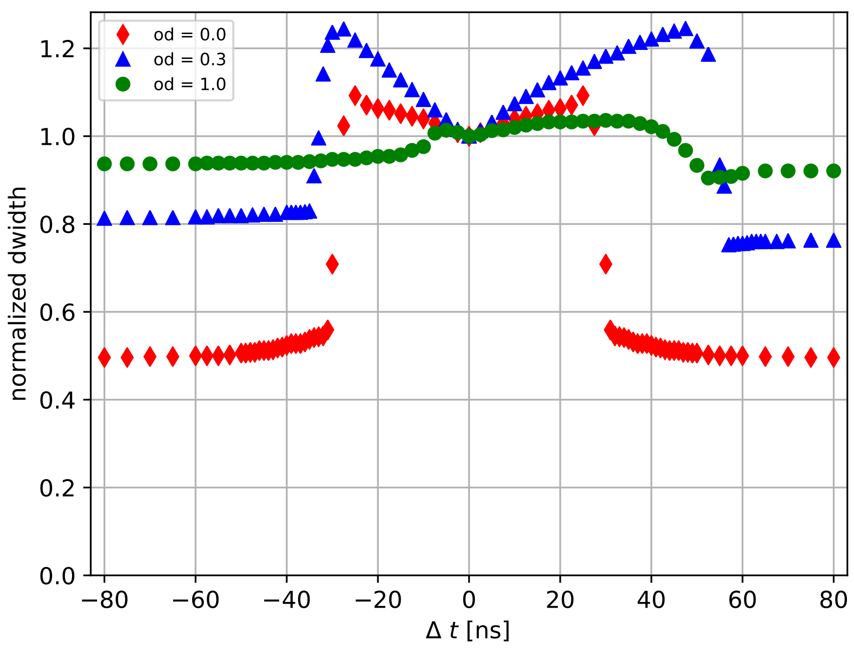

Figure IV.10.: Median values of w_d for the different scenarios in the non-linear regime analyzed with FCEventReconstructor of November 11, 2019. Here, all curves follow the shapes they had in the last version of FCTraceAnalyser and even better. I.e. does the blue curve not drop dramatically at $\Delta t \approx 60\,\text{ns}$.

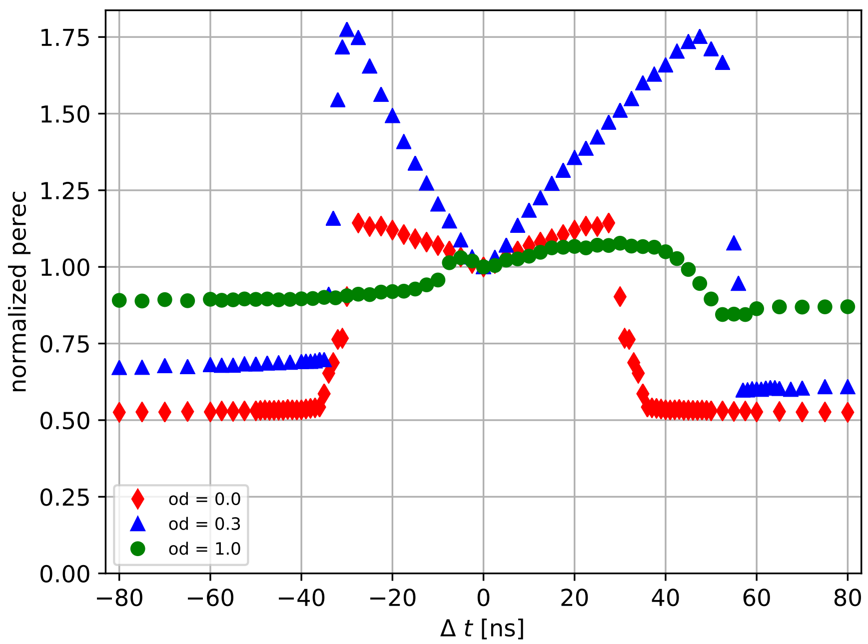

Figure IV.11.: Median values of pe_{rec} for the different scenarios in the non-linear regime analyzed with FCEventReconstructor of November 11, 2019. The data points are, as they can be expected from Figure IV.10.

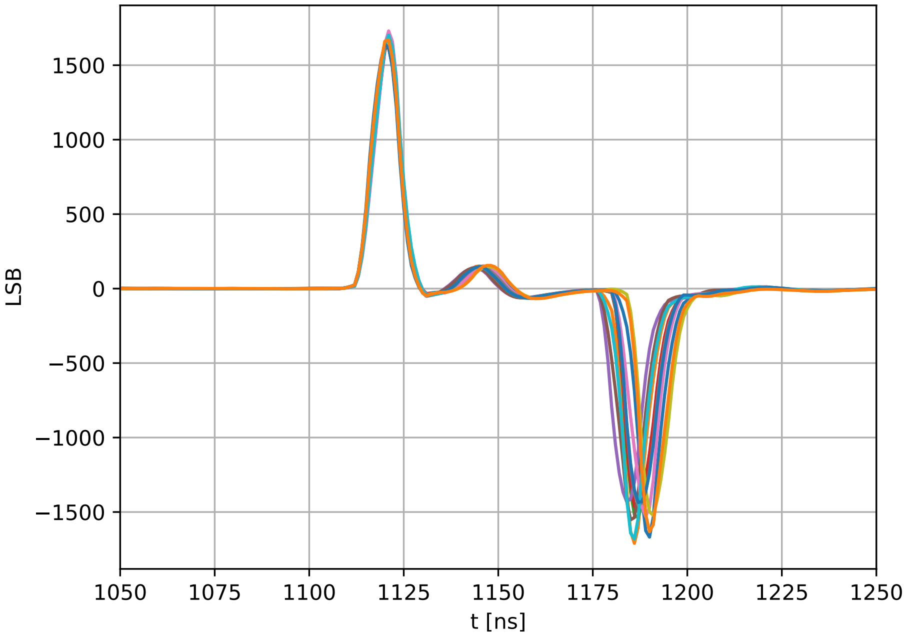

Figure IV.12.: Differentiated traces of one event with the od03 scenario in the non-linear regime at $\Delta t = 0\,\mathrm{ns}$

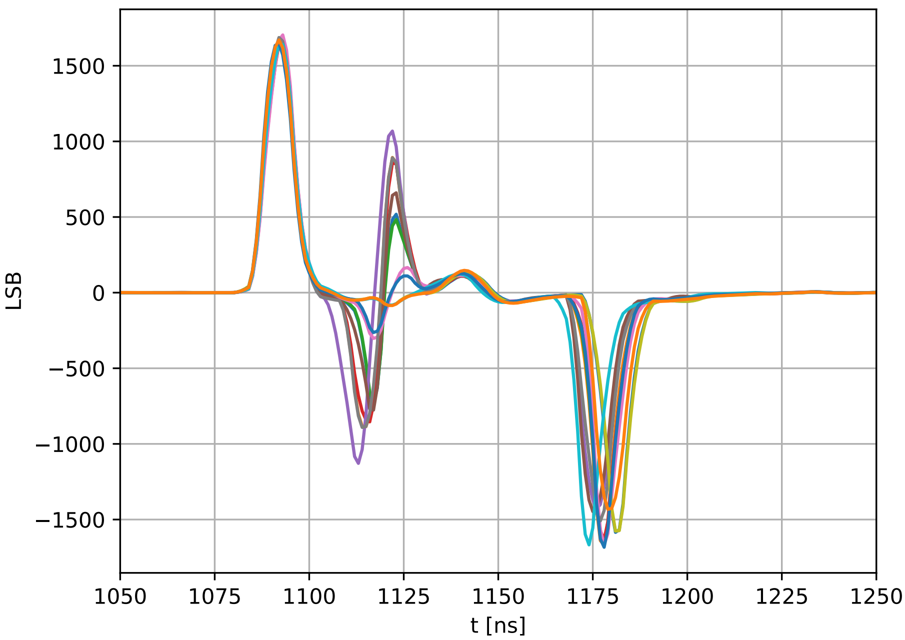

Figure IV.13.: Differentiated traces of one event with the od03 scenario in the non-linear regime at $\Delta t = -30\,\mathrm{ns}$

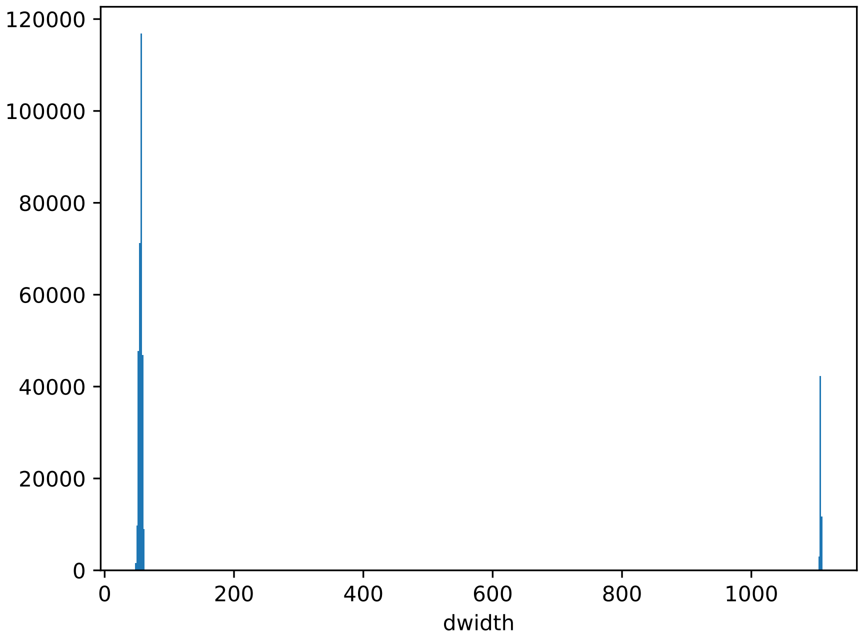

Figure IV.14.: Histogram of w_d in od10 scenario in the non-linear regime at $\Delta t = -25\,\mathrm{ns}$ analyzed with FCEventReconstructor from November 11, 2019. More than 1/6 of the measurements is obviously too high, due to a malfunction of the reconstruction.

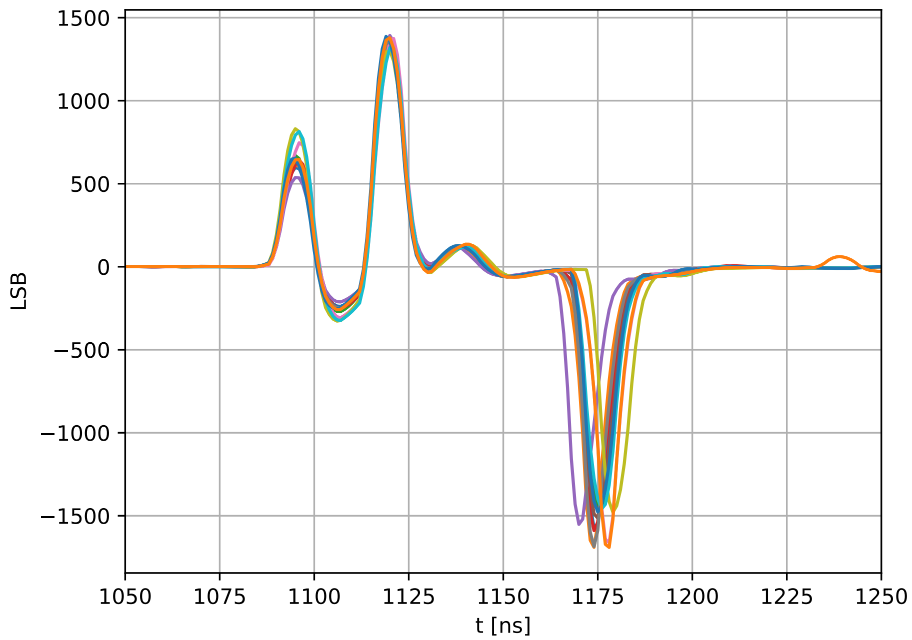

Figure IV.15.: Differentiated traces of one event with the od10 scenario in the non-linear regime at $\Delta t = -25\,\mathrm{ns}$

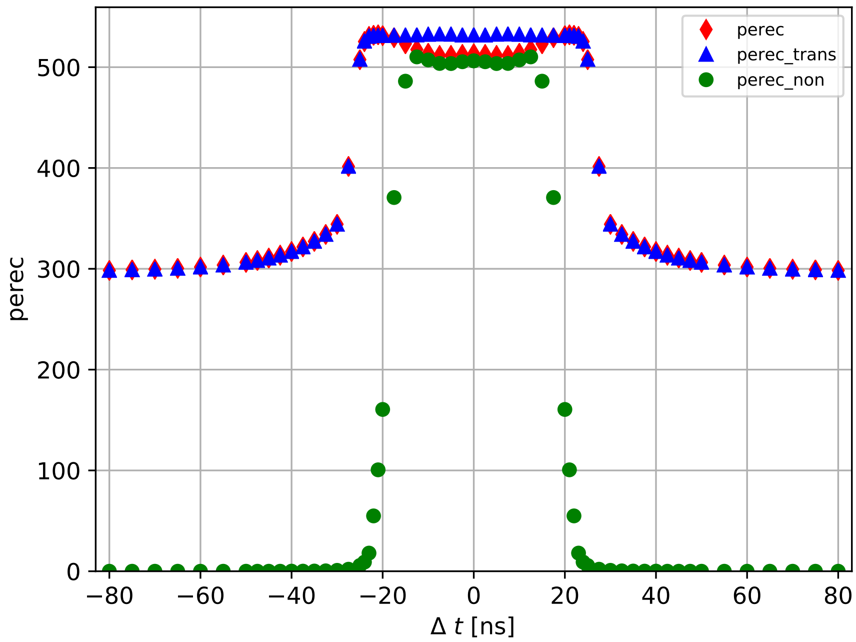

Figure IV.16.: Total reconstructed number of p.e. with reconstruction methods of the transition regime and the non-linear regime for the od00-scenario in transition regime analyzed with FCEventReconstructor of November 11, 2019. Contrary to the previous version, the curve for pe_{rec} now follows mostly the curve for $pe_{\mathrm{rec,tans}}$ and is only little affected by $pe_{\mathrm{rec,non}}$ between $\Delta t <$ 15 ns. For $|\Delta t| \geq 20$ ns, the curve of pe_{rec} is hidden behind the curve of $pe_{\mathrm{rec,trans}}$.

and in Figure IV.13. A histogram of w_d in the od10 scenario in the non-linear regime at $\Delta t = -25$ ns is plotted in Figure IV.14 and the corresponding differentiated trace is shown in Figure IV.15. Finally, in Figure IV.16 pe_{rec} in the transition regime in the od00 scenario is displayed.

Figure IV.9 shows that the calculation of w_d, contrary to the previous version, mostly reproduces FCTraceAnalyser for the od00 scenario and the od03 scenario. Figure IV.10 shows that for the od10 scenario more than half of the data points reproduce FCTraceAnalyser, although there are new issues for $\Delta t < 0$ ns. When looking at the median values of the reconstructed intensity in units of pe_{rec} one finds that the curve follows the shape of the curve for w_d. The more dramatic increase of the values, especially in the od03 scenario, is due to the exponential reconstruction in the non-linear regime. The expected limits (in units of pe_{rec}) are reached quite well: the od00 scenario decreases to 0.53, the od03 scenario drops to 0.67 (left) and 0.61 (right) and the limits of the od10 scenario are 0.89 (left) and 0.87 (right).

For the series of measurements recorded in the non-linear regime, there are two issues. The average values in the od10 scenario at $\Delta t < 0$ ns exceed to normalized reconstructed intensities in units of $w_d$of more than 3.5. Secondly, there is an increase of the normalized reconstructed intensities in all scenarios around $\Delta t = 0$ ns instead of the constant plateau that was expected in Section III.3. This has been already observed with FCTraceAnalyser and will be discussed first.

To understand why the curves in the non-linear regime calculated by FCTraceAnalyser as well as FCEventReconstructor show the previously mentioned linear increase for data points around $\Delta t = 0$ ns it is useful to consider the differentiated traces. Figures IV.12 and IV.13 show those for the od03 scenario at $\Delta t = 0$ ns and at $\Delta t = -30$ ns. This scenario is chosen because it shows the highest reconstructed intensities; the Δt is chosen because the normalized w_d reaches its maximum there.

The following should happen when calculating w_d in this scenario: At $\Delta t = 0$ ns FCEventReconstructor finds the maximum of the differentiated trace at about 1200 ns. Then, to the right of it, a minimum is searched. To not consider the local minimum before the small local maximum around 1150 ns[57] a threshold is implemented. It states that any maximum of the differentiated trace must be at least a certain fraction of the global maximum to be considered. In consequence, the minimum to calculate w_d is the global minimum and is found at about 1185 ns. With that w_d can be calculated to be 67.3 ns. At $\Delta t = -30$ ns the local maximum and minimum in between the global maximum and minimum should be considered. Then, two w_d should be calculated.[58] Finally, only the larger one should be considered. This would be smaller than the one found at $\Delta t = 0$ ns and therefore indicate that the pulses can partially be separated.

However, what actually happens for $\Delta t = -30$ ns is that the local maximum and minimum are not considered since the maximum apparently is below the threshold. Therefore, for the calculation of w_d only the global maximum and the global minimum are considered. This leads to the value found, being $w_d = 83.2$ ns. The conclusion can be driven that in these measurements the second maximum is too weak to pass the threshold that was introduced to suppress the inevitable, local maximum mentioned previously.

For the od10 scenario at $\Delta t < 0$ ns the problem seems to be mostly in the average since in the data using the median only a small increase to values larger than 1 can be found. The histogram in Figure IV.14 shows the distribution of the reconstructed intensity in

[57]This peak appears always and must therefore be omitted.

[58]From the global maximum to the local minimum (≈ 25 ns) and from the local maximum to the global minimum (≈ 55 ns)

units of w_d in the od10 scenario, measured in the non-linear regime at $\Delta t = -25$ ns. This measurement is chosen because the average of its normalized w_d is the largest (3.78), as can be seen in Figure IV.9. As the histogram shows, most values of w_d ($\approx 80\%$) are of the expected order of magnitude, being about 55 ns. This corresponds to a normalized w_d of 0.94. However, the histogram also shows that there is a significant amount of data points at more than 1100 ns, corresponding to a normalized w_d of almost 19. The differentiated trace of that measurement (see Figure IV.15) shows that there might be two peaks, but only one minimum be detected. The (falsely) returned w_d is 1160 ns, which could correspond to the last point in the differentiated trace that is =0 before the minimum. However, this needs to be examined in more detail by the responsible developers for a future version of FCEventReconstructor.

In the transition regime the reconstruction of the intensity in units of pe_{rec} improved, too. As stated in Section IV.1 the calculation of A_{1200} already works well with the first version of FCEventReconstructor. However, in that version pe_{rec} followed the values obtained with the reconstruction algorithm of the non-linear regime, due to the non-existing non-linear threshold and the poor calculation of w_d. As it can be seen in Figure IV.16, this could be improved in the current version of the software. For $|\Delta t| > 20$ ns $pe_{rec,non}$ is zero and therefore, the reconstructed intensity in units of pe_{rec} only follows the algorithm for the transition regime. Unfortunately for $|\Delta t| \leq 20$ ns the old problem still is unresolved. $pe_{rec,non}$ is still lower than $pe_{rec,trans}$ and therefore causes a dip for $|\Delta t| < 20$ ns in pe_{rec}. By regarding the normalized reconstructed intensity in units of pe_{rec} the conclusion can be driven that the reconstruction in transition regime itself is correct: At the edge of the measurement the normalized value of $pe_{rec,trans}$ is 0.56 while the normalized value of pe_{rec} is 0.58. The former must be regarded as better. It is closer to the expected limit of 0.5 as well as to the limits found in the linear regime and in the non-linear regime, being 0.53 (linear) and 0.54 (non-linear). For future versions of FCEventReconstructor this measurement should be taken into account to either find a more proper calibration or to implement a higher non-linear threshold. Correct reconstruction would be characterized by a plateau for the reconstructed intensity as described in Section III.3 and as obtained with the reconstruction algorithm for the transition regime.

IV.2.2. Measurements with NSB

As mentioned in Chapter III measurements with night-sky background of different levels, simulated by a blue LED, were performed for all measurements. However, it turned out that the effect of NSB to these measurements is marginal. Therefore, only one series of measurements is presented and discussed here, being the od00 scenario in the transition regime. For all the other series of measurements, the results are qualitatively the same.

Figure IV.17 shows the absolute values of the reconstructed intensity in units of pe_{rec} for the whole series of measurements. This includes NSB levels of 0 MHz, 3 MHz, 300 MHz and 1500 MHz. The series with 0 MHz is equal to the series of measurements in the transition regime previously presented. One can see that with increasing NSB-level the reconstructed intensity decreases.

In Chapter II it is stated that the most relevant part are delays with $|\Delta t| < 10$ ns, as this is the typical duration of an air shower. Figure IV.18 shows a more closely zoomed in look at the series of measurements with delays up to $|\Delta t| = 20$ ns. This higher resolution can be used for a more detailed analysis. Initially, a comparably large change in the reconstructed intensity was expected when switching on the LED. This would be between the red (0 MHz) and the blue (3 MHz) curve. As the plot shows, this is not the

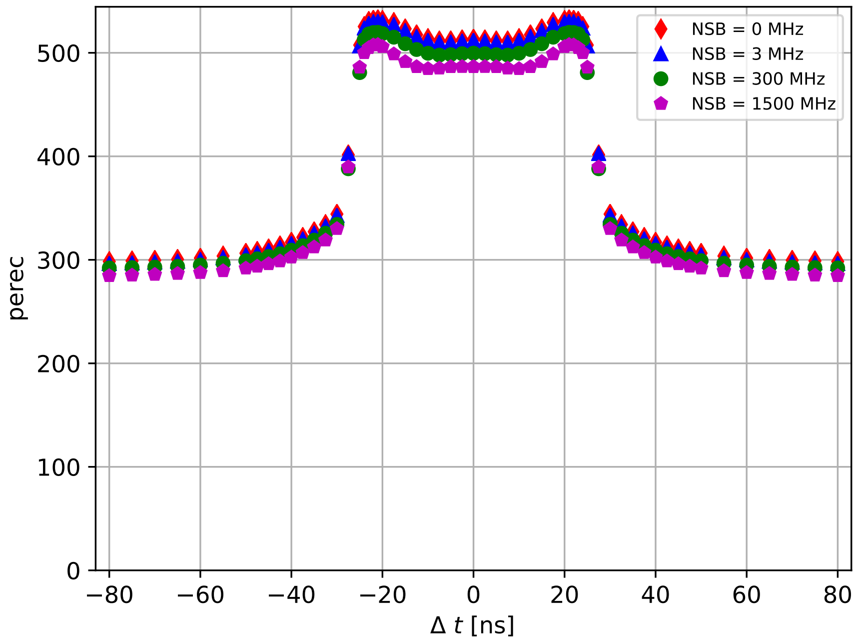

Figure IV.17.: Absolute values of pe_{rec} of several series of NSB measurements with the od00 scenario in the transition regime, analyzed with FCEvent-Reconstructor of November 11, 2019. With increasing NSB-levels, the reconstructed number of p.e. decreases.

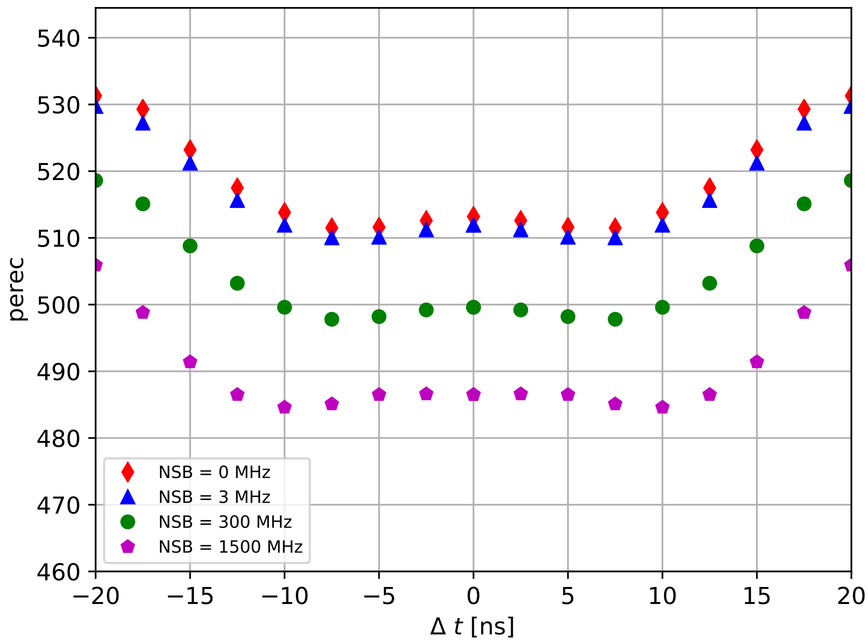

Figure IV.18.: Zoom into a zone around $\Delta t = 0\,\text{ns}$ of the plot above. The effect of NSB is clearly below 10%.

case.

Two steps can be found: one from 3 MHz to 300 MHz and one from 300 MHz to 1500 MHz. The latter is trivial, since the NSB-level increased by more than 1 GHz. However, the first one is more astonishing since the increase is an order of magnitude less than in the second case and the NSB is expected to effect the measurement linearly.

The shapes of the curves remain unchanged for all levels of NSB. The total dependance of a measurement can be estimated by comparing the reconstructed intensity from a data point with NSB =0 MHz and a data point with NSB =1500 MHz. The latter is a realistic value for an observing night. E.g. at $\Delta t = 0$ ns, $pe_{\text{rec}} = 513$ for no NSB and $pe_{\text{rec}} = 487$ for NSB =1500 MHz. Therefore, one can conclude that a realistic NSB decreases the reconstructed intensity in units of pe_{rec} by about 5%. Most likely this is a reconstruction issue and can be corrected for in future versions of FCEventReconstructor.

IV.3. Discussion

This section covers two major points: First, it is summarized why the algorithms for reconstructing the intensity are mostly sufficient in their current form and in which cases they are not. Second, ideas are presented on how to improve the software in each regime.

In the linear regime reconstruction mostly works as intended as stated in Section IV.1. However, when calculating pe_{rec} there is still the issue that between $16\,\text{ns} \leq \Delta t \leq 20\,\text{ns}$ a value for the background is determined by using the maximum in this time interval. This causes the reconstructed intensity in units of pe_{rec} to be too low in an interval of 10 ns – 30 ns. Nevertheless, this does not need to be regarded as a serious issue. The typical duration of a shower at one position is of the order of 1 ns. Therefore, it must not be expected that photons from the same shower arrive more than 10 ns after the first photon. For comparably weak showers which are reconstructed in the linear regime this is all the more valid. From this one can conclude that the only possibility to observe something like $|\Delta t| > 10$ ns in the linear regime would be two showers in close succession. However, this would only be a serious issue if the patterns formed by the two showers would be at exactly the same position. This could be the case when the two initial photons would arrive at the same time from the same direction, i.e. the same source. Even though this might be studied deeper with simulations it is an unlikely scenario, considering the typical photon flux at TeV-energies.

As already mentioned a relatively easy way to improve the reconstruction algorithm for pe_{rec} in the linear regime would be to consider the median value of the pz-corrected trace inside a larger time interval to estimate the background. However, from Figure I.10 we know that a pz-corrected pulse in the linear regime lasts for about 30 ns.[59] Therefore, to make sure a second pulse would not interfere with the measurement at all, at least the time interval from 16 ns to 76 ns needs to be considered. This works only under the assumption that there is no third pulse reaching the camera in the same interval.

In the transition regime the only thing to improve is the dip around $\Delta t = 0$ ns and the small peaks around $\Delta t = \pm 20$ ns, respectively. Both are an issue in the reconstruction of the intensity in units of pe_{rec}. However, the peaks are just about 5% higher than the dip. Further, it again is very unlikely that a scenario leading to one of the peaks appears during actual observations, for the same reasons as above.

The easiest way to improve these evaluations would be to increase the non-linear threshold. This would make the non-linear reconstruction algorithm start to work at higher number of p.e. and therefore at higher w_{d}, when the value of $pe_{\text{rec,non}}$ has in-

[59] Meaning that from the moment when the value increases above the baseline, towards the moment the baseline is reached again, 30 ns pass.

creased stronger than the value of $pe_{\mathrm{rec,trans}}$. However, it must be ensured that the reconstruction of the intensity in units of pe_{rec} here is not going to be tailored to this specific scenario.

In the non-linear regime there is still need for improvements. Due to the exponential behavior of the intensity in the non-linear regime even small deviations in units of w_{d} lead to strong deviations in units of pe_{rec}. Instead of the expected plateau the normalized value of pe_{rec} increases to 1.20 at $\Delta t = -10\,\mathrm{ns}$ and 1.18 at $\Delta t = 10\,\mathrm{ns}$. Such deviations are not acceptable. However, the question of such a scenario's likeliness must be asked again.

A strong shower lasting for about 10 ns would indeed be possible. Nevertheless, it would be a constant illumination instead of two light flashes as in the Two-Laser-Experiment. As of yet, such a long lasting illumination was not systematically investigated. In any case the differentiated trace will have another shape as those displayed in Figure IV.13 or in Figure IV.15 and therefore the algorithm will calculate different values for w_{d}. To investigate the response of FlashCam on a constant illumination for about 10 ns, simulations should be taken into account or even future experiments are needed.

Until these simulations are performed it should be tried to improve the software using the measurements available. In particular, the reconstruction should be stabilized. Especially such excessive values, as displayed on the right edge in Figure IV.14, should be avoided. To achieve this, the global maximum and minimum should be considered in the calculation of w_{d} if the standard calculation delivers a value higher than this. Further, the threshold for finding a local maximum/minimum should be lowered. By doing so, such features would be considered in the calculations more often. This should affect the calculations in such a way that of the two laser pulses in the measurements only one is going to be considered at lower Δt as of now.

V. Suggestions for an Experiment for the Astrophysics Advanced Lab-Course

While studying physics at the University of Tübingen students not only have to follow lectures. Basics of laboratory work are taught during three obligatory laboratory courses in the bachelor's program to all physics students. When specializing towards an experimental field usually one more specialized laboratory course must be taken additionally. The individual experiments are structured in such a way that the students first learn about the topic on their own with an experiment script. At the day of the experiment they are instructed by a supervisor to realize the measurements. Finally, a protocol must be drawn up in which the theory and the measurement results are summarized and evaluated. Usually, the students work together in groups of two.

This all is valid also for the specialization in Astronomy and Astrophysics, as well as for the international *Master Astro and Particle Physics*, where the *Astrophysikalisches Fortgeschritte-nen-Praktikum*[60] must be attended. In the course students can choose from several experiments/tasks from computational astrophysics, astronomy and detector development. As of yet, TeV gamma-astronomy is not represented there, although it is one of the largest projects at IAAT according to the number of people assigned. However, with the setups presented, a well understood experiment on which measurements can easily be performed is available. In this chapter ideas what students could learn during such a laboratory experiment (Section V.1) and which measurements could be performed (Section V.2) are presented.

V.1. The Students' Learning Goals

As already indicated above, learning in a lab course experiment is split in two parts. The first being the theoretical part, done by reading the script and by explanations from the supervisor. In the script it is common to include some questions / easy exercises the students have to answer/solve on their own and are tested on the day of the experiment. The second part is the practical work of performing and evaluating the experiment. Subsequently, the two parts also target different topics. While the theoretical part is used to teach the physics behind the experiment and the observing technique, the practical part gives an idea of the actual experimental work and the procedure of data analysis.

The theoretical part of an experiment concerning CTA needs to address two major topics. One being Cherenkov astronomy, the other being the technology behind it. To waken the students' interest Cherenkov astronomy should be discussed first. A historical summary, starting with the first detection of extraterrestrial gamma rays in 1967 by the US military and including major successes, such as the first IACT telescope at Mt. Whipple and the H.E.S.S. experiment, is suggested as an introduction. In the same section different interesting sources should be mentioned. A meaningful selection is left to data analysts, knowing these sources better than the author of this thesis. However, the Crab Nebula, GRBs and other very high energetic events should be used to trigger the students' interest in the topic. The end of this part should be an outlook to the upcom-

[60]German for *advanced laboratory course in astrophysics*

ing Cherenkov telescope array. Although the experiment is dedicated to ground-based gamma astronomy, satellites such as CGRO and FERMI should be mentioned. At the same time, it can be explained why it is not feasible to observe at energies above some 10 GeV with satellites (the flux is very low and the area of an satellite is very limited).

Next, the Cherenkov effect should be explained, together with the IACT. A phenomenological explanation of the effect, rather than the complete theoretical derivation is suggested. However, for interested students a reference to a textbook, such as [Lon11] should be given. After the explanation of the Cherenkov effect, the requirements for suitable instruments should be understood. Therefore, the technical aspects should be discussed next. At the example of FlashCam the working principle of a modern camera for Cherenkov telescopes can be explained. Especially the working principle of a PMT should be mentioned since detection methods are not adequately covered in other courses.[61] Depending on what is done in the experimental part, one could go into more detail for one or more special topics. Such could be the estimation of the gain based on [Bel94], if SPE-measurements are performed at the day of the experiment. For further developing of the experiment script, the inclusion of other detection methods and telescope setups (such as Schwarzschild-Couder mounted telescopes for example) is possible.

As an exercise the students could calculate the area on the ground (in some given altitude) that is covered by a Cherenkov cone.[62] Further, they could be asked where on this area the most Cherenkov photons can be found. As a task concerning the technical aspects, students could estimate the number of electrons at the end of a PMT, based on the assumption of one photo-electron hitting the first dynode and a specified gain per dynode. A scientific question that could be posed very well might be why the IACT concentrates on gamma-photon induced showers and discriminates particle showers. It has to be ensured that the answers to those questions/exercises are not directly given in the script. However, there should be sufficient information in it to answer/solve them.

On the day of the experiment, the theory should be deepened with the supervisor. The answers should be reviewed and the experimental setup should be explained. Of course, a description of the experiment must be included into the script, too. However, it is always easier to understand a setup in vito. After that, measurements can be performed and evaluated. In this part, the students get an impression of daily lab work. They learn about the practical application of the topics presented in the theoretical part and evaluating measurements. Evaluation at the day of the experiment itself might only cover those steps that require special scripts and programs such as FCEventReconstructor. Their handling must be given and explained in the script. Further evaluation could be left as a homework when writing the protocol. Detailed suggestions concerning the practical part are given in Section V.2.

The protocol should include a short summary of the theory, particularly with regard to the answers of the questions. Further, all measurements and their results should be presented. A description of the setup, however, should be omitted: the experience from other laboratory courses shows that such a description mostly is a duplicate of the description given in the script.

V.2. Implementation of the Experiment

The suggestion for the start of the actual experiment is to perform an SPE measurement. To see the influence of the light intensity on this measurement, it should be realized at

[61] Opinion of the author

[62] It has to be elaborated how many parameters should be given and which they have to find on their own.

different intensities.[63] Directly afterwards the evaluation can be performed using fc-utils programs and Python scripts. Applying the knowledge from the theoretical part the students should be able to find the best SPE measurement, considering the plots of the fitted PM-response function on the spectra. To show a realistic process of measuring and finding parameters the determined gain per pixel should be later used in the *BuildTable.py*-script to create unique configuration values for each group.

The task was given to evaluate if the Two-Laser-Experiment could be meaningfully included into a lab course experiment. Firstly, it has to be stated that performing a series of measurements as presented in this thesis is not feasible in the lab course. Performing and evaluating would cost too much time. However, measurements with the Two-Laser-Setup at individual Δt could be considered as a possible option. Such would allow for the same didactic goals (as measuring complete series of measurements) while leaving time for other aspects: By regarding the traces (a Python script for easy plotting exists), digital signal processing could be explained and the changes in the reconstructed intensity would be easy understandable. Therefore, it can be stated that measurements with the Two-Laser-Setup can be meaningfully included into a future lab course experiment. However, as of yet this is only one option among others.

Part of this discussion must also be, whether the transition regime and the non-linear regime should be mentioned or not. On the one hand, these regimes are a main feature of FlashCam. The non-linearity for high intensity inputs in combination with the fully digital signal processing is what makes FlashCam unique. However, care must be taken to not confuse the students with too much content. Since most of them might come into contact with (digital) signal processing for the first time it might be already exhausting to follow the explanations when considering the linear regime only. Subsequently, it is suggested to exclude the transition regime and the non-linear regime from the experiment for the beginning. If it turns out that students frequently ask what happens at high intensities or that the experiment is too small, this could still be included. It might also be thinkable to include information about these regimes into an additional part of the experiment script which needs not be worked through on a mandatory basis.

It is recommended to perform a test run to evaluate the final concept before offering the experiment to all participants of the lab course. For this test run, either a volunteering group during a upcoming lab course or volunteering students from the institute (who are not familiar with FlashCam) should be chosen.

[63] In this case, a single p.e. is no longer measured. However, the PM-response function also can be fitted (with restrictions) to multi p.e. distributions.

VI. Conclusions and Outlook

The goal of this thesis was to determine the response of FlashCam on light pulses of a length that is typical for gamma ray induced air showers, being a few nanoseconds.

To achieve this an experiment with two pulsed lasers was set up in a darkbox. Using a pulse generator and different delay-lines, the lasers were triggered with temporal delays between 0 ns and 80 ns[64] in steps of 0.5 ns to 5 ns and with an accuracy better than 0.1 ns. The functionality of the setup was validated in several measurements.

While performing the measurements three scenarios have been realized, being characterized by different settings of the laser intensities relative to each other. The ratios have been 1:1, 2:1 and 10:1. They were realized by attenuating one of the lasers with optical filters. In the linear regime and the non-linear regime, measurements in all these scenarios have been performed. Further, measurements in one scenario (od00) have also been performed in the transition regime.

Having clear expectations concerning the results (*detected intensity* against the *temporal delay* of the pulses), the measurements could be used to test and improve a new version of a FlashCam analysis program (*FCEventReconstructor*), which includes the whole analysis chain in one program for the first time. In the linear regime, the maximum of the pz-corrected trace *pzmax* is the parameter chosen to determine the detected intensity. It behaved as expected for different Δt. Therefore, the reconstructed intensity in units of pe_{rec} in this regime mostly met the expectations. However, a numerical relict appeared at $\Delta t \approx 20$ ns.

Initial issues in the reconstruction of the intensity in the non-linear regime and the transition regime have been identified and could be strongly improved, using the results of the respective measurements and evaluations. However, there are still issues that should not exist. For $|\Delta t|$ being around 0 ns and up to 30 ns w_{d}, increases almost proportionally to $|\Delta t|$.[65] Following w_{d} exponentially pe_{rec} also increases instead of being constant as expected for these Δt.

As a next step it must be clarified if there is a significant likelihood to observe events that are comparable to the measurements in which the reconstruction shows issues not acceptable. To achieve this, further discussions should be triggered as well as shower simulations taken into account. Once this is done, it has to be discussed which of the issues are too unlikely to happen so they can be ignored and for which the reconstruction code needs to be improved. However, one has to be careful to not optimize the code for these artificial scenarios. It must remain sufficiently flexible to correctly respond to different events in actual observations.

The measurements have been realized with different levels of background illumination, too. However, it turned out that this illumination does not affect the results qualitatively. However, a quantitative change was found: the reconstructed intensity in units of p.e. decreased by about 5%.

The methods developed for easy evaluation of multiple measurements as well as the setup itself will be used for an experiment in the *Astrophysikalisches Fortgeschrittenen-Praktikum*. Suggestions which topics an experiment concerning FlashCam/CTA should

[64] 80 ns is the largest Δt realized. Technically, up to 102.5 ns would be possible with the setup presented.

[65] The upper limit for Δt depends on the intensity and could be even higher.

cover, and which measurements could be performed were presented. Future work on this topic includes writing a complete script for the experiment and to finally discuss which measurements are feasible and didactically useful. Before the experiment can finally be included to the laboratory course it has to be evaluated by a volunteering group.

Finally, it can be stated that the goal of the thesis was reached. Measurements at different intensities and with different delays were performed. The data recorded helped to better understand FlashCam and to debug the analysis software. Since the reconstruction of the intensity is not yet fully satisfactory, suggestions were made how to further improve the software. Upcoming versions of FCEventReconstructor will again be tested with the measurements recorded in the framework of this thesis until a properly working reconstruction software is ready.

A. Signal Processing Circuits

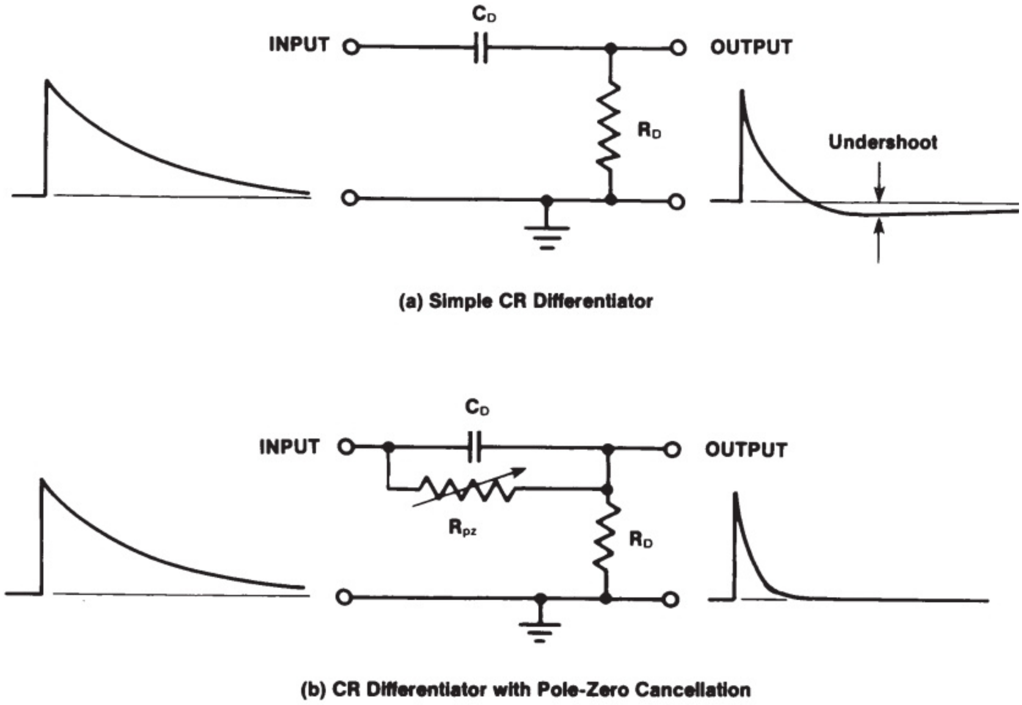

Figure A.1.: CR Differentiator circuit and CR Differentiator with pole-zero cancellation circuit. On the left an example for an incoming signal and on the right the resulting output are shown. The most remarkable advantage of the pz-cancellation is the non-existence of an undershoot and therefore shorter signals. Image: [Ort20]

B. Further information about the devices used

Wavelength (± 10) [nm]	Type (LDH-)	Pulse* (FWHM) [ps]	Max rep rate [MHz]	High avg. power** [mW]	Low avg. power*** [mW]	CW power [mW]
266 (± 3)	P-FA-266	Please see separate data sheet for LDH-P-FA Series.				
355 (± 3)	P-FA-355	Please see separate data sheet for LDH-P-FA Series.				
375	P-C-375	< 40	40	2.0	0.8	--
	P-C-375B	< 40	40	4.0	0.8	--
	D-C-375	< 40	40	4.0	0.8	10
	P-C-375M	< 90	40	10.0	2.5	--
	D-C-375M	< 90	40	10.0	2.5	50
395	P-C-390	< 70	40	5.0	1.0	--
	D-C-390	< 70	40	5.0	1.0	30
405	P-C-405	< 50	80	4.0	0.8	--
	P-C-405B	< 50	40	3.0	1.0	--
	D-C-405	< 50	40	3.0	1.0	50
	P-C-405M	< 90	40	25.0	10.0	--
420	P-C-420	< 70	40	5.0	0.5	--
	D-C-420	< 70	40	5.0	0.5	30
440	P-C-440	< 80	40	2.0	0.4	--
	P-C-440B	< 80	40	4.0	0.8	--
	D-C-440	< 80	40	4.0	0.8	50
	P-C-440M	< 100	40	25.0	10.0	--
	D-C-440M	< 100	40	25.0	10.0	200
450	P-C-450	< 100	40	2.0	0.5	--
	P-C-450B	< 70	40	5.0	0.7	--
	D-C-450	< 70	40	5.0	0.7	10
455	P-C-450M	< 90	40	20.0	4.0	--
	D-C-450M	< 90	40	20.0	4.0	200
470	P-C-470	< 80	40	3.0	0.6	--
	P-C-470B	< 70	40	4.0	0.8	--
	D-C-470	< 70	40	4.0	0.8	60
	P-C-470M	< 120	40	20.0	8.0	--
	D-C-470M	< 120	40	20.0	8.0	200
485	P-C-485	< 110	40	2.0	0.4	--
	P-C-485B	< 90	40	5.0	0.7	--
	D-C-485****	< 90	40	5.0	0.7	50
500	P-C-500	< 130	40	2.0	0.5	--
	P-C-500B	< 100	40	5.0	0.7	
	D-C-500	< 100	40	5.0	0.7	40
510	P-C-510	< 130	40	2.0	0.3	--
	P-C-510B	< 110	40	4.0	0.6	--
	D-C-510****	< 110	40	4.0	0.6	40
515 (± 3)	P-FA-515L	Please see separate data sheet for LDH-P-FA Series.				
520	P-C-520	< 130	40	2.5	0.7	--
	D-C-520****	< 130	40	2.5	0.7	20
	P-C-520M	< 160	40	25.0	6.0	--
532 (± 3)	P-FA-530B/L/XL	Please see separate data sheet for LDH-P-FA Series.				
532 (± 3)	D-TA-530	< 70	80	0.7	0.3	10
	D-TA-530B	< 70	80	1.1	0.5	20
557 (± 3)	P-FA-560	Please see separate data sheet for LDH-P-FA Series.				
561 (± 3)	D-TA-560	< 80	80	0.5	0.3	5
	D-TA-560B	< 70	80	0.7	0.5	20
594 (± 3)	D-TA-595	< 80	80	0.3	0.2	5
	D-TA-595B	< 80	80	0.5	0.4	5

Figure B.1.: Extract of the data-sheet for the PicoQuant LDH laser series. The marked lines indicate the two lasers used. Source: [Pic19].

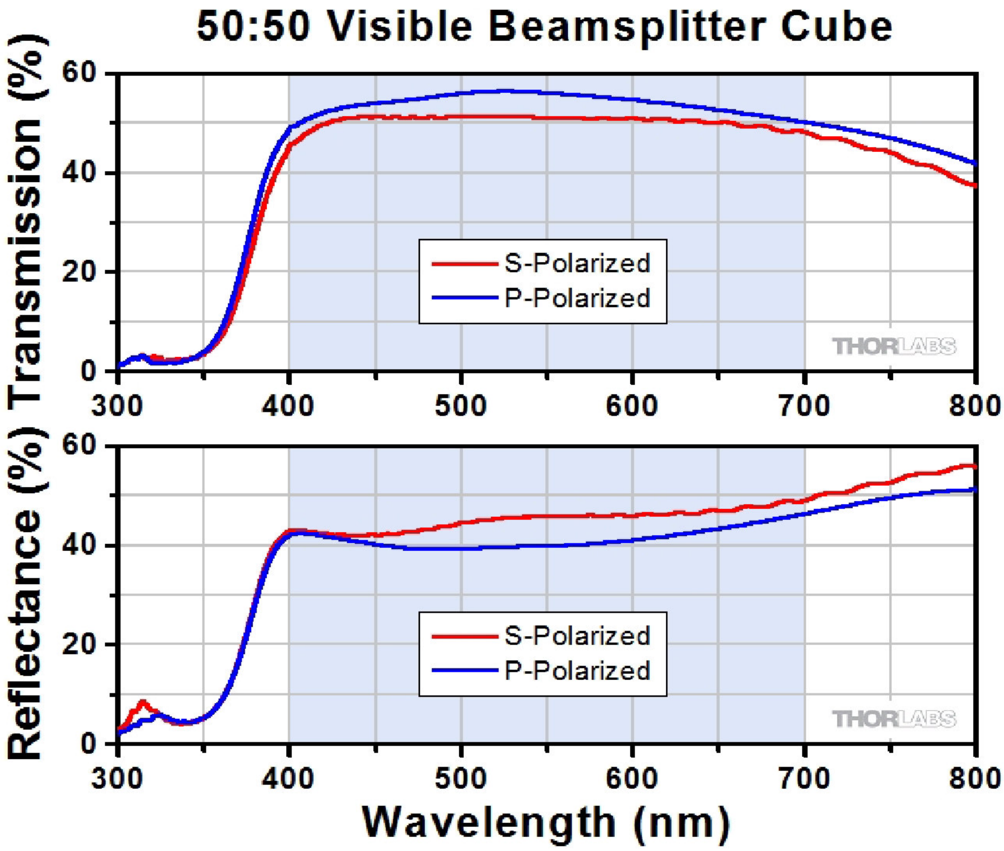

Figure B.2.: Transmission and Reflectance of the beam-splitter-cube BS016 used in the Two-Laser-Setup as function of the wavelength. Image: [Tho19]

Table B.1.: A list of all externally bought devices used in the Two-Laser-Setup. Devices not listed here were custom-made at IAAT or other member institutes of the FlashCam-group.

Device	Manufacturer	Serial Number
Beam Splitter Cube	Thorlabs	BS016
Diffuser	Thorlabs	ED1-C20-MD
Driver Innsbruck	PicoQuant	PDL 820 (PDL Sepia II)
Driver Tuebingen	PicoQuant	PDL 800-D
Laser Innsbruck	PicoQuant	LDH-P-C-440B
Laser Tuebingen	PicoQuant	LDH-D-C-405
ND-Filter-Wheel	Thorlabs	NDC-50C-4M-A
ND-Filter	Thorlabs	NDUV2R03A (respective 10A, 20A)
NSB-LED	Nichia	NSPB510AS
Optical Bench	Thorlabs	MB1560/M
Optical Rail	Thorlabs	RLA300/M
Oscilloscope	Agilent-Infiniium	DSO8104A
Photodiode (PD)	ALPHALAS	UPD-500-UD
Power Supply	Telemeter Electronic	PL303QMT-P
Pulse Generator	Agilent	33250A
Servo-Motor	ROBOTICS CO.	Dynamixel MX28-AT

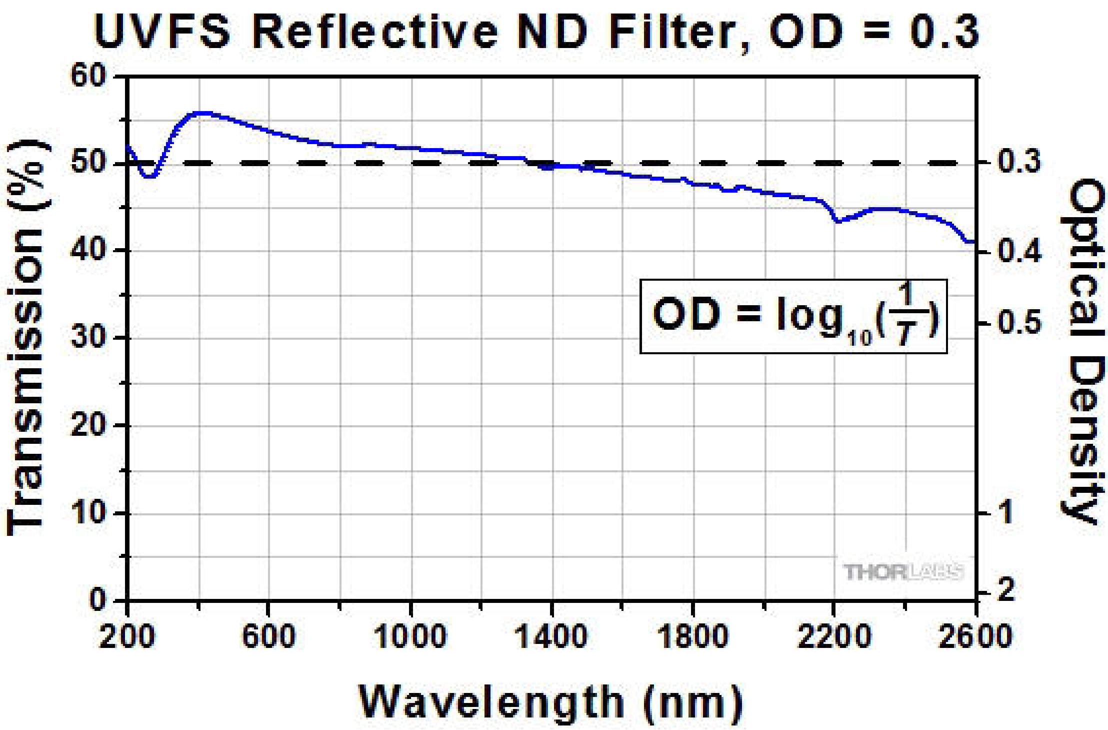

Figure B.3.: Transmission-wavelength diagram of the od03-filter. At wavelengths $\sim$ 400 nm the transmission is about 55% instead the nominal 50% (dashed line). Image: [Tho19]

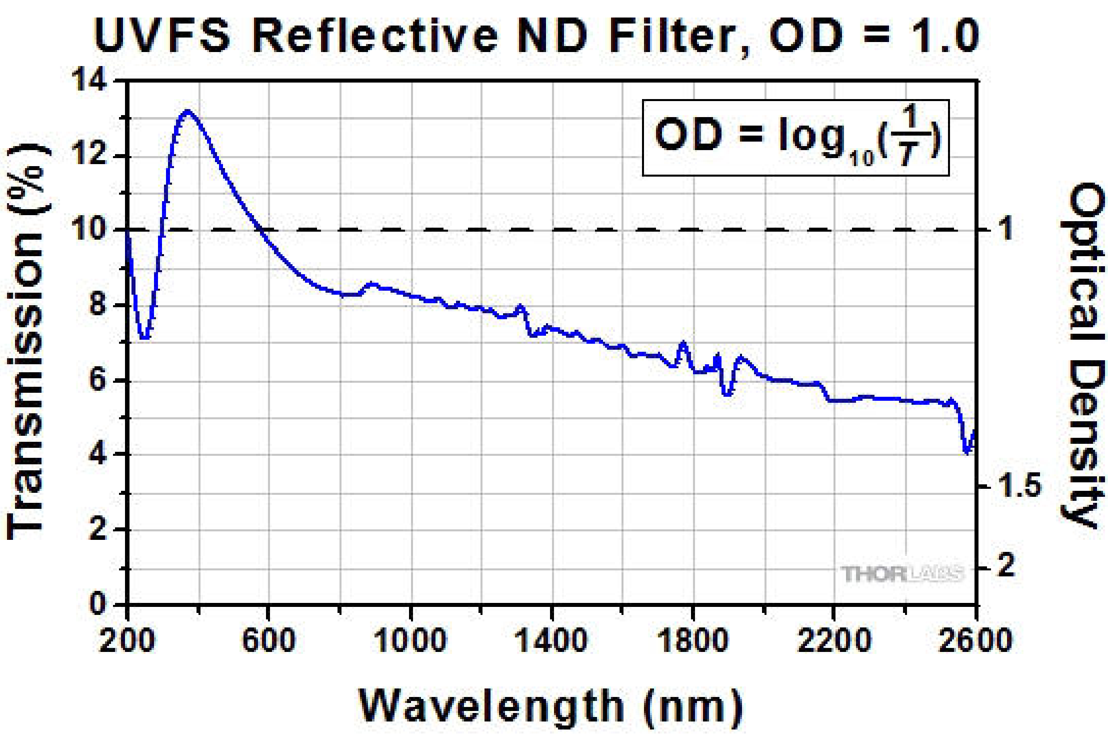

Figure B.4.: Transmission-wavelength diagram of the od10-filter. At wavelengths $\sim$ 400 nm the transmission is about 11% – 13% instead of the nominal 10% (dashed line). Image: [Tho19]

C. Configuration values used during evaluation

Table C.1.: The channel-dependent configuration values used in FCEventReconstructor. The values for pz-correction (*pz*) were determined earlier and are therefore given with only four decimal places.

channel	pz	ugain	pzgain	area_gain	b1_offset	b2_offset
00	0.7507	8.389426	5.053363	0.028491	7.483275	6.997433
01	0.7448	7.967597	4.804748	0.028930	7.481263	7.064688
02	0.7470	7.948229	4.786937	0.028321	7.482389	7.021578
03	0.7443	7.630631	4.609753	0.029128	7.479470	7.040608
04	0.7474	7.613268	4.575382	0.026887	7.415629	7.059670
05	0.7451	8.066476	4.877339	0.029052	7.473241	7.071868
06	0.7419	8.540275	5.169371	0.031127	7.529568	7.062342
07	0.7495	8.382502	5.054306	0.029399	7.505460	7.044028
08	0.7522	8.473607	5.135887	0.031356	7.551342	7.055329
09	0.7442	7.950694	4.796374	0.030460	7.517617	7.078483
10	0.7441	8.639107	5.285564	0.033818	7.574203	7.105720
11	0.7417	8.436988	5.108757	0.030143	7.523886	7.036970

Table C.2.: Configuration values that are (assumed to be) constant over all channels. Whilst the first six values are calculated, the other ones are assumptions, either found during earlier calibrations or only have minor impact.

Parameter	Value
rbgtopz	$3.503418 \cdot 10^{-1}$
area_offset	$9.200998 \cdot 10^{2}$
b1_scale	$-3.255974 \cdot 10^{-4}$
b2_scale	$-5.206390 \cdot 10^{-4}$
c1	$2.336152 \cdot 10^{-2}$
c2	$3.300958 \cdot 10^{-2}$
gain_reftemp	$3.000000 \cdot 10^{1}$
gain_tempcoeff	$-5.000000 \cdot 10^{-3}$
gain_refnsb	0.000000
gain_nsbcoeff	$3.000000 \cdot 10^{-2}$
bl_shift	$2.000000 \cdot 10^{2}$
linear_limit	$2.500000 \cdot 10^{3}$
transition_threshold	$2.800000 \cdot 10^{3}$
transition_limit	$4.500000 \cdot 10^{1}$
nonlinear_threshold	$2.000000 \cdot 10^{1}$

In this appendix, the configuration values used to run FCEventReconstructor in its final version are presented. The values that were determined for each channel independently are shown in Table C.1. Since the setup consists of only twelve pixels some values were estimated and/or assumed to be constant. These are shown in Table C.2. The non-assumed values from both tables can be obtained with the script *BuildTable.py* by Baiyang Bi.

D. Additional Information for the Lab Course Experiment

In the following, a possible table of contents for the script for the lab course experiment is presented. Below that, the scripts and fc-utils programs are listed that are needed to perform SPE- and Δt-measurements.

1. Very High Energetic Gamma-Rays
   - Sources
   - Why are Space-Based Missions Unrealistic
   - Cherenkov Effect
   - Electromagnetic vs. Hadronic Showers
2. Ultra Low Level Light Detection
   - Photo-Electron Multiplier Tubes (PMTs)
   - Silicon Photomultiplier (SiPM)
3. Imaging Air Cherenkov Technique
   - Working principle
   - Cherenkov Telescopes
   - FlashCam
   - Other Detection Methods of Very High Energetic Particles
4. The Experiment
   - Origin and Goal
   - Setup
5. Measurements
   - SPE Measurements
   - (Δt) Measurements
6. Evaluation
   - Evaluation of SPE measurements
   - Evaluation of (Δt) Measurements
   - Further Evaluation at Home

Scripts to be used for evaluations

To evaluate an SPE-measurement, the *FCEventReconstructor* has to be run with the output file of the measurements first. As configuration values default values should be used to give the students a realistic impression. Those could be 8 for *ugain* and 5 for *pzgain*.

The other channel-dependent values (*area_gain*, *b1_offset* and *b2_offset*) are needed in the transition regime and the non-linear regime only. Therefore, they are not relevant here. However, the best choice is to just run the script *BuildTable.py* with the default gains introduced above.

The output file of FCEventReconstructor has to be processed further with the Python script *EvtsRec2ParameterDir.py*. This creates a directory containing files for each channel in which the measured values of one parameter from all events are listed. Here, the parameter one is interested in is *umax*. These files must be passed in succession to the program *FCSPEFit* (to be found in the fc-utils), together with a file containing boundary conditions and a path to save the output containing the fitted parameters. This can be done with the script *SPEFit.py*.

Finally, the whole directory (now containing the files with the measured values for each channel and the SPE-fits) must be passed to the script *PlotSPEFitUmax.py*, which plots the spectra (being the measured values) together with fitted the PM-response function and saves them in the directory.[66] Considering the plots, the students can determine which measurement delivered the best fit and therefore, which gains are the most reliable. To receive the values for *pzgain*, Equation 8 must be considered after the values for *pzmax* are extracted with the EvtsRec2ParameterDir.py-script.

To evaluate "'normal"' measurements the programs listed in *Masterscript.py* must be run in succession with the command line options given there. The programs themselves are explained in Section III.2

[66] PlotSPEFitUmax.py requires the SPE-fit-files to have the ending *.dat* and the files with the values for *umax* to end with *.txt* – SPEFit.py puts the correct endings automatically.

E. List of Abbreviations

Table E.1.: A list of all used abbreviations. Note that an "‘s"’ at the end indicates the plural of the abbreviated word/term.

A_{1200}	Area of the upsampled trace above 1200 LSB
a.s.l.	Above sea level
CE	Collection efficiency
CTA	Cherenkov Telescope Array
DAQ	Data aquisition system
DE	Detection efficiency
dwidth	See "‘w_d"’
FADC	Flash analog-to-digital converter
FPGA	Field programmable gate array
HV	High voltage
IAAT	Institut für Astronomie und Astrophysik Tübingen
IACT	Imaging Air Cherenkov Technique
KSP	Key Science Project
LST	Large-Sized telescope
MPIK	Max-Planck-Institut für Kernphysik
MST	Medium-Sized telescope
nd	Neutral density
NSB	Night-sky background
od	Optical density
PDP	Photon detector plane
PD	Photo diode
p.e.	Photo-electron(s)
pe_{rec}, perec	Reconstructed number of p.e.
PM	Photo-electron multiplier, Photomultiplier
PMT	Photo-electron multiplier tube, Photomultiplier tube
pz	Pole-zero
QE	Quantum efficiency
ROS	Readout electronics
SiPM	Silicon photo-multiplier
SPE	Single photo-electron
SST	Small-Sized telescope
w_d	Width of the differentiated trace
WR	White Rabbit

List of Figures

Bibliography

[Ach13] Acharya et al. Introducing the CTA concept. *Astroparticle Physics*, 43:3–18, March 2013.

[Agi13] Agilent Technologies. *Infiniium 8000 Series Oscilloscopes – Superior mixed-signal analysis and debug*, December 2013.

[Aha04] Aharonian. *Very High Energy Cosmic Gamma Radiation. A Crucial Window on the Extreme Universe*. World Scientific Publishing Co. Pte. Ltd., Singapore, 2004.

[ALP19] ALPHALAS GMBH. *Ultrafast Photodetectors – UPD Series*, August 2019.

[Bel94] Bellamy et al. Absolute calibration and monitoring of a spectrometric channel using a photomultiplier. *Nuclear Instruments & Methods in Physics Research*, 339:468–476, 1994.

[Bie17] Biegger. Optimization of a pulse generator for the evaluation of CTA FlashCam readout electronics and development of a calibration chamber for detector testing. Master's thesis, Eberhard Karls Universität Tübingen, 2017.

[CTA19a] `https://www.cta-observatory.org/`, 2019. Accessed: December 6, 2019.

[CTA19b] CTA Consortium. *Science with the Cherenkov Telescope Array*. World Scientific Co.Pte.Ltd., 2019. Open-access, doi: 1709.07997.

[de 15] de Naurois, Mazin. Ground-based detectors in very-high-energy gammay-ray astronomy, November 2015.

[Hal02] Halzen, Hooper. High-energy neutrino astronomy: the cosmic ray connection. *Reports on Progress in Physics*, 65:1025–1078, 2002.

[HES19] `https://www.mpi-hd.mpg.de/hfm/HESS/`, 2019. Accessed: January 27, 2020.

[ISD18] `http://www.isdc.unige.ch/cta/outreach#Analysis?en`, 2018. Accessed: August 20, 2018.

[Kre98] Krennich et al. Stereoscopic observations of gamma rays at hte whipple observatory. *Astroparticle Physics*, 8:213–221, 1998.

[Len12] Lena, Rouan, Lebrun, Mignard. *Observational Astrophysics*. Springer Verlag, Heidelberg, Germany, 3 edition, 2012.

[Lon11] Longair. *High Energy Astrophysics*. Cambridge University Press, Cambridge, United Kingdom, 2011.

[Ort20] `https://www.ortec-online.com/-/media/ametekortec/other/amplifier-introduction.pdf?la=en`, 2020. Accessed: January 27, 2020.

[Pic19] `https://www.picoquant.com/`, 2019. Accessed: August 16, 2019.

[Pue15] Puehlhofer et al. FlashCam: a fully digital camera for the medium-sized telescopes of the Cherenkov Telescope Array. In *34th International Cosmic Ray Conference (ICRC2015)*, volume 34 of *International Cosmic Ray Conference*, July 2015.

[Pue19] Puehlhofer et al. FlashCam: a fully digital camera for the Cherenkov telescope array medium-sized telescopes. In Stephen L. O'Dell and Giovanni Pareschi, editors, *Optics for EUV, X-Ray, and Gamma-Ray Astronomy IX*, volume 11119, pages 530 – 536. International Society for Optics and Photonics, SPIE, 2019.

[Ryb04] Rybicki, Lightman. *Radiative Processes in Astrophysics*. Wiley-VCH Verlag GmbH & Co.KGaA, Weinheim, Germany, 2004.

[Sal18] Salzmann. Commissioning of a Night-Sky-Background Light Source for the IAAT CTA-FlashCam Test Setup, 2018. Bachelor's thesis, Eberhard Karls Universität Tübingen.

[SEN19] `https://www.sense-pro.org/lll-sensors/pmt`, 2019. Accessed: December 10, 2019.

[Sta14] `http://large.stanford.edu/courses/2014/ph241/alaeian2/`, 2014. Accessed: November 28, 2019.

[Tho19] `https://www.thorlabs.com/`, 2019. Accessed: July 10, 2019.

[Wat11] Alan A. Watson. The discovery of cherenkov radiation and its use in the detection of extensive air showers. *Nuclear Physics B - Proceedings Supplements*, 212-213, Mar 2011.

Acknowledgments

This work would not have been possible without the help and advice of many people. I would like to thank everyone who contributed in any way to the success of my Master's thesis.

I thank Prof. Andrea Santangelo for the possibility to work in the High-Energy-Astrophysics group and for all his lectures that enforced my will to become an astrophysicist and accompanied me throughout my whole time at university. I thank Dr. Sebastian Diebold for introducing me to FlashCam, for proofreading my thesis and answering all my questions with great patience and knowledge. I also thank Dr. Gerd Pühlhofer for his ideas and explanations throughout the whole time I worked on this thesis as well as for the proofreading. I thank Dr. Baiyang Bi for his help with the analysis programs and in the laboratory. Further thanks go to the FlashCam team for the warm welcome and the ideas regarding my measurements. I also want to thank the whole IAAT and especially my office colleagues Inga, Christian and Heiko for a fun and inspiring working atmosphere. Finally, I thank Georg Stadelmann for proofreading the language of my thesis.

Additionally to the people mentioned above I want to thank Dr. Chris Tenzer for his advice and especially for introducing me to Python and for wakening my interest in hardware development during my Bachelor studies.

I also want to thank all the friends I met during the past years in Tübingen, especially: Dani, Georg, Lena, Max and Raffa.[67] It is always a pleasure and I hope we can stay in touch for many more years. Further, I want to say thanks to my clubs and sports-teams for encouraging me, offering distraction from physics and keeping me down-to-earth: The Musikverein "'Echo"' Renfrizhausen, the HSG Neckartal, the CVJM Hagelloch and the University Teams of Handball and Hockey.

Finally, my greatest thanks go to my parents who supported me throughout my whole life and made all this possible. Without them I would not have become who I am.

[67] If you didn't realize: I don't want to make a statement with the order, I've just sorted you in alphabetically :D